Wang et al. Virology Journal 2012, 9:106
http://www.virologyj.com/content/9/1/106

VIROLOGY JOURNAL

RESEARCH Open Access

PA from an H5N1 highly pathogenic avian influenza virus activates viral transcription and replication and induces apoptosis and interferon expression at an early stage of infection

Qiang Wang[1,2†], Shijian Zhang[2,3,4†], Hongbing Jiang[2], Jinlan Wang[2], Leiyun Weng[2], Yingying Mao[2], Satoshi Sekiguchi[5], Fumihiko Yasui[5], Michinori Kohara[5], Philippe Buchy[6], Vincent Deubel[6], Ke Xu[1], Bing Sun[1] and Tetsuya Toyoda[2,5,7*]

Abstract

Background: Although gene exchange is not likely to occur freely, reassortment between the H5N1 highly pathogenic avian influenza virus (HPAIV) and currently circulating human viruses is a serious concern. The PA polymerase subunit of H5N1 HPAIV was recently reported to activate the influenza replicon activity.

Methods: The replicon activities of PR8 and WSN strains (H1N1) of influenza containing PA from HPAIV A/Cambodia/P0322095/2005 (H5N1) and the activity of the chimeric RNA polymerase were analyzed. A reassortant WSN virus containing the H5N1 Cambodia PA (C-PA) was then reconstituted and its growth in cells and pathogenicity in mice examined. The interferon promoter, TUNEL, and caspase 3, 8, and 9 activities of C-PA-infected cells were compared with those of WSN-infected cells.

Results: The activity of the chimeric RNA polymerase was slightly higher than that of WSN, and C-PA replicated better than WSN in cells. However, the multi-step growth of C-PA and its pathogenicity in mice were lower than those of WSN. The interferon promoter, TUNEL, and caspase 3, 8, and 9 activities were strongly induced in early infection in C-PA-infected cells but not in WSN-infected cells.

Conclusions: Apoptosis and interferon were strongly induced early in C-PA infection, which protected the uninfected cells from expansion of viral infection. In this case, these classical host-virus interactions contributed to the attenuation of this strongly replicating virus.

Keywords: Influenza virus, PA, Transcription, Replication, Apoptosis, Interferon

* Correspondence: toyoda_tetsuya@yahoo.co.jp
†Equal contributors
[2]Units of Viral Genome Regulation, the Key Laboratory of Molecular Virology & Immunology, Institut Pasteur of Shanghai, Chinese Academy of Sciences, 411 Hefei Road, 200025, Shanghai, P. R. China
[5]Department of Microbiology and Cell Biology, Tokyo Metropolitan Institute of Medical Biology, 3-18-22 Honkomagome, Bunkyo-Ku, Tokyo 113-8613, Japan
Full list of author information is available at the end of the article

Background

Influenza A viruses cause disease in humans, pigs, other mammals, and birds [1]. The genomes of influenza A viruses are composed of 8 negative-sense single-stranded RNA segments; this segmented genome allows gene reassortment between viruses in co-infected cells to produce new viruses. Reassortment of influenza A virus genes caused the deadly H2N2 "Asian flu" and the H3N2 "Hong Kong flu" pandemics in 1957 and 1968, respectively. During these pandemics, the avian virus PB1, HA and NA, or PB1 and HA genes, respectively, were introduced into circulating human viruses [2,3]. The last pandemic strain, the novel swine-origin influenza virus A/H1N1 (S-OIV), carries PB2 and PA genes of avian origin [4]. In addition to the S-OIV pandemic flu, H5N1 highly pathogenic avian influenza viruses (HPAIV) have caused severe or fatal disease in humans in Asia, the Middle East, and Africa since their emergence in Hong Kong in 1997 (WHO, http://www.who.int/csr/disease/avian_influenza/en/). The H5N1 influenza virus ribonucleoprotein complex (RNP) contributes to viral pathogenesis in chickens [5,6]. Influenza viruses with high polymerase activity have also shown high pathogenicity [7,8]. These lines of evidence suggest that the influenza RNA-dependent RNA polymerase (RdRp) contributes to its pathogenesis.

Influenza A virions contain 8 negative-sense single-stranded RNA genome segments and RdRp [9]. Genome segments 1, 2, and 3 encode the RdRp subunits PB2, PB1, and PA, respectively. Segment 4 encodes hemagglutinin (HA), segment 5 nucleoprotein (NP), segment 6 neuraminidase (NA), segment 7 matrix protein 1 (M1) and an ion channel (M2), and segment 8 non-structural protein 1 (NS1) and nuclear export protein (NEP). A second open reading frame of segment 2 encodes PB1-F2 in some strains.

The RdRp subunit PB1 is the core subunit of the RdRp complex and mediates RNA polymerization [10-12], while PB2 is the cap-binding subunit [13-15] and PA has cap-dependent endonuclease activity [16-20]. Influenza virus RdRp catalyzes both transcription of viral mRNA and replication of the viral genome. Influenza transcription is a prototype of primer-dependent initiation. The viral RdRp binds to the cap-1 structures of host mRNAs and cleaves off 9 to 15 nucleotides to generate primers for viral transcription, a process known as "cap snatching" [13,21-23]. The internal initiation mechanism of influenza virus genome replication was recently elucidated [24,25].

H5N1 HPAIV does not efficiently adapt to transmission to humans [26]. However, once it does infect humans, it results in high mortality of approximately 60% [27,28]. Although some genomic combinations, such as those between human H3N2, avian H5N1, and horse H7N7 or between human H3N2 and avian H2N2, may be incompatible [29-32], reassortment between H5N1 HPAIV, which is epizootic among poultry almost worldwide [33], and currently circulating human influenza viruses, including the pandemic S-OIV and seasonal influenza viruses (H1N1 and H3N2), is one of the most important potential threats for the next pandemic. Kashiwagi *et al.* recently reported that the PA of H5N1 HPAIV activated the polymerase activity by enhancing promoter binding [34]. Multiple functions of PA in addition to promoter binding, such as transcription and replication [9,18], endonuclease activity [16,17,19,20,35], cap binding [19], protease activity [36], proteolysis induction [37], pathogenesis in mice [38], and thermal sensitivity of RNP [39], have been identified.

In this paper, we describe the activation of the polymerase activity of A/Puerto Rico/8/1934 (PR8, H1N1) and A/WSN/1933 (WSN, H1N1) RNPs by the H5N1 HPAIV PA of A/Cambodia/P0322095/2005, which was isolated from a Cambodian victim [40], and the reconstitution of the chimeric virus to analyze the effect of this H5N1 PA in the background of WSN, a well-studied mouse influenza infection model. We found a discrepancy between the viral polymerase activity and proliferation efficiency in cells and its pathogenesis in mice. We then analyzed the mechanism of the attenuation and the low pathogenicity of WSN carrying H5N1 PA.

Results

Effect of H5N1 Cambodia PA on the PR8 and WSN replicons and *in vitro* RdRp activity

We first examined the replicon activity in 293 T cells of a chimeric PR8 RNP containing H5N1 Cambodia PA (Figure 1A). Influenza replicon activity was measured as previously described [41,42]. The replicon activity was about 200.0 ± 8.2% that of the PR8 RNP (Student's *t*; $p < 0.005$), while the Cambodia RNP showed 43.8 ± 2.9% of the replicon activity of the PR8 RNP ($p < 0.005$). The expression of RdRp and NP in the transfected cells was confirmed by western blotting (Additional file: Figure S1).

As we found 2-fold activation of the PR8 replicon by H5N1 Cambodia PA, we purified both PR8 RdRp and a chimeric RdRp (PR8PB2-PR8PB1-H5N1 Cambodia PA) in order to investigate the effect of the H5N1 Cambodia PA on RdRp activity *in vitro*. Sodium dodecyl sulfate-polyacrylamide gel electrophoresis (SDS-PAGE) showed that H5N1 Cambodia PA migrated to a higher position than did PR8PA; the Cambodia PA band almost overlapped with that of 18 × HisPR8PB2 (Figure 1B). The identity of H5N1 Cambodia PA was confirmed by western blotting against PA (Figure 1C).

We next compared the activities of the purified RdRps *in vitro*. We tested the transcription activity using v84 and globin mRNA primers (Figure 1D and E, mRNA), and replication activity using v84 and c84 with and

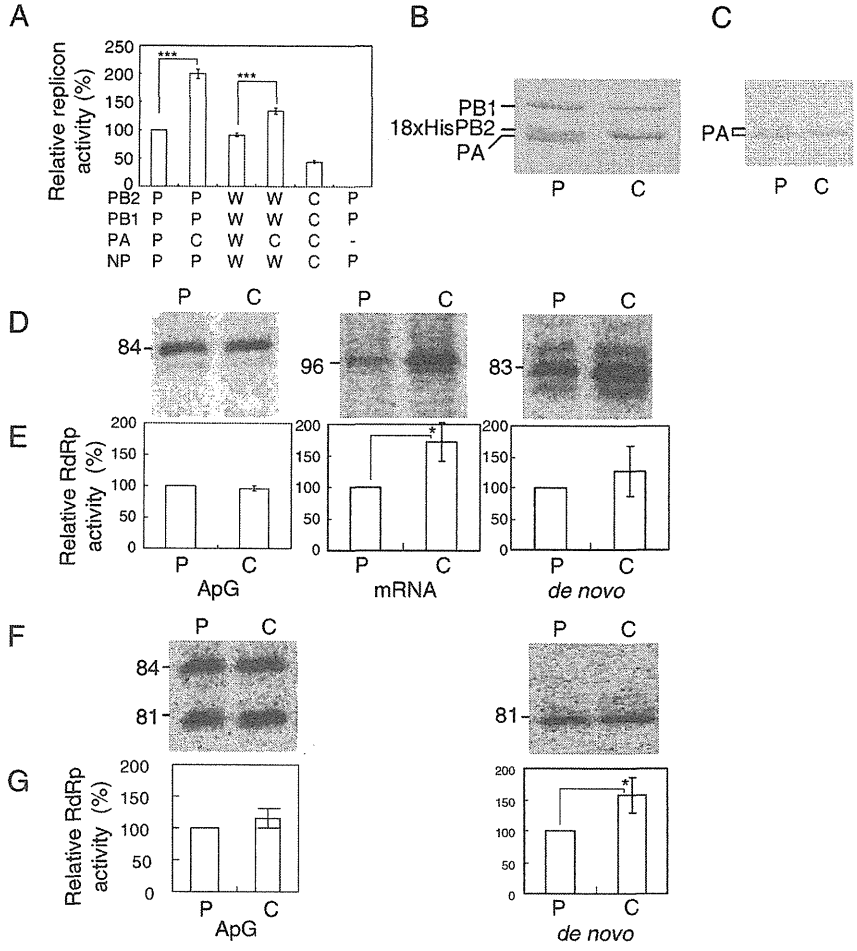

Figure 1 Replicon and *in vitro* RNA-dependent RNA polymerase (RdRp) activities of the chimeras of H5N1 Cambodia PA with PR8 and WSN. A: Replicon activity of the chimeric influenza virus ribonucleoproteins (RNPs) of WSN and PR8 with H5N1 Cambodia PA. The relative replicon activities of WSN and PR8 with H5N1 Cambodia PA in 293 T cells were compared with those of WSN and PR8. The combination of PB2, PB1, PA, and NP is indicated below the graph. W, WSN; P, PR8; C, H5N1 Cambodia. As a negative control, PR8 replicon without PA was used. **B:** Purified influenza virus PR8 RdRp (P) and PR8PB2-PR8PB1-C-PA RdRp (C). Each RdRp (5 pmol) was subjected to sodium dodecyl sulfate-polyacrylamide gel electrophoresis (SDS-PAGE) on 7.5% gels and Coomassie brilliant blue staining. The positions of PB1, 18×His-PB2, and PA are indicated on the left. **C:** Western blot of the purified influenza virus chimeric RdRp. Each RdRp (5 pmol) was electro-blotted onto the nitrocellulose membrane. The PA was detected by western blotting with anti-PA antibodies. The position of PA is indicated on the left. **D** and **E:** Comparison of the chimeric RdRp activities in *in vitro* transcription and replication of v84 with those of PR8. The v84 model template RNA (200 nM) was transcribed by PR8RdRp (P) or PR8PB2-PR8PB1-C-PA RdRp (C) with or without (*de novo*) 0.1 mM ApG (ApG) or 0.5 μg globin mRNA (mRNA). **F** and **G:** Comparison of chimeric RdRp activity in *in vitro* replication of c84 with that of PR8. The c84 model template RNA was incubated with or without ApG (*de novo*). Products were analyzed by PAGE on 6% gels containing 8 M urea and the images analyzed with a Typhoon Trio plus. Examples of the images are shown in D and F. The size of the product RNA is indicated on the left. The mean and standard deviation (error bar in the graph) of the polymerase activity relative to that of PR8 RdRp were calculated from 2 independent measurements of 3 different RdRp preparations. Statistical significance was evaluated with Student's *t*-test. *$p < 0.05$, ***$p < 0.005$.

without the dinucleotide primer ApG (Figure 1D, E, F, and G). ApG-primed and *de novo* initiation of v84 transcription produced 84- and 83-nt products, respectively, while globin mRNA-primed transcription produced 96-nt products. Because virion RdRp uses 10–15 nucleotide primers to initiate from the C at the 2nd position from the 3′ end of the genome [18,22], the 96-mer products were assigned to the transcripts from the 13th G next to the 12th U of the cap-1 structure (m^7GmACACUUGCUUUU) of rabbit β-globin mRNA (GenBank; M10843). The mean and standard deviation (error bar in the graph) of the polymerase activity relative to that of PR8 RdRp were calculated from 2 independent measurements of 3 different RdRp preparations. The relative

ApG-primed replication activity of the chimeric RdRp was 95.9 ± 4.5% of that of PR8 RdRp, while its *de novo* replication activity was 126 ± 40% of that of PR8 RdRp. The chimeric RdRp produced 171 ± 31% ($p < 0.05$) of the amount of 96-nt transcription products. ApG-primed initiation of c84 produced 84- and 81-nt products, while *de novo* initiation produced 81-nt products. The relative replication activity of ApG-primed initiation of c84 by the chimeric RdRp was 116 ± 16% of that by PR8 RdRp, while its *de novo* initiation was 156 ± 29% of that by PR8 RdRp ($p < 0.05$). We thus confirmed that H5N1 Cambodia PA enhanced both the transcription and replication activities of PR8 RdRp.

Before reconstituting WSN carrying H5N1 Cambodia PA, we tested the effect of H5N1 Cambodia PA on the WSN replicon (Figure 1A). WSN replicon activity (91.3 ± 3.2%) was similar to that of PR8. The replicon activity of WSN containing the H5N1 Cambodia PA (which was 133.9 ± 5.8% of that of the PR8 replicon) was about 1.5-fold higher than that of the WSN replicon ($p < 0.005$). Therefore, we also observed an activation effect of H5N1 Cambodia PA on the WSN replicon.

Effect of H5N1 Cambodia PA on virus growth in MDCK cells, chicken embryo fibroblasts (CEF), and Vero cells

Next, we tested whether the RdRp activation effect of H5N1 Cambodia PA affected virus growth. As the RdRp subunits of PR8 and WSN are highly homologous, with 96, 97, and 98% amino acid identity between the PB2, PB1, and PA genes, respectively, and as the activation effect of H5N1 Cambodia PA was confirmed in both the WSN and PR8 replicons, we used a WSN reconstitution system to analyze the effect of H5N1 Cambodia PA in H1N1 virus. The WSN virus carrying H5N1 Cambodia PA (C-PA) was reconstituted successfully. First, we compared the multi-step growth of C-PA with that of WSN in MDCK, CEF, and Vero cells.

In MDCK cells, the C-PA titer was always lower than that of WSN and plateaued ($4.7 \pm 0.2 \times 10^4$ PFU/mL) 16 hr post-infection (pi), while the WSN titer was $2.2 \pm 0.03 \times 10^5$ PFU/mL 16 hr pi and plateaued ($5.6 \pm 1.6 \times 10^6$ PFU/mL) 36 hr pi (Figure 2A). The C-PA titer in MDCK cells 60 hr pi was significantly higher than that of WSN ($p < 0.001$). The titers of C-PA and WSN in CEF did not plateau even 60 hr pi. However, the C-PA titer 60 hr pi ($7.1 \pm 1.4 \times 10^5$ PFU/mL) was about half of that of WSN ($1.3 \pm 0.4 \times 10^6$ PFU/mL), a statistically significant difference ($p < 0.001$, Figure 2B). We therefore observed a discrepancy between the effects of H5N1 Cambodia PA on RdRp activity and on virus growth in MDCK and CEF cells. However, the C-PA titer in Vero cells between 24 hr and 60 hr pi was significantly higher than that of WSN ($p < 0.05$, Figure 2C). Both titers plateaued at $5.6 \pm 0.1 \times 10^5$ PFU/mL 70 hr pi.

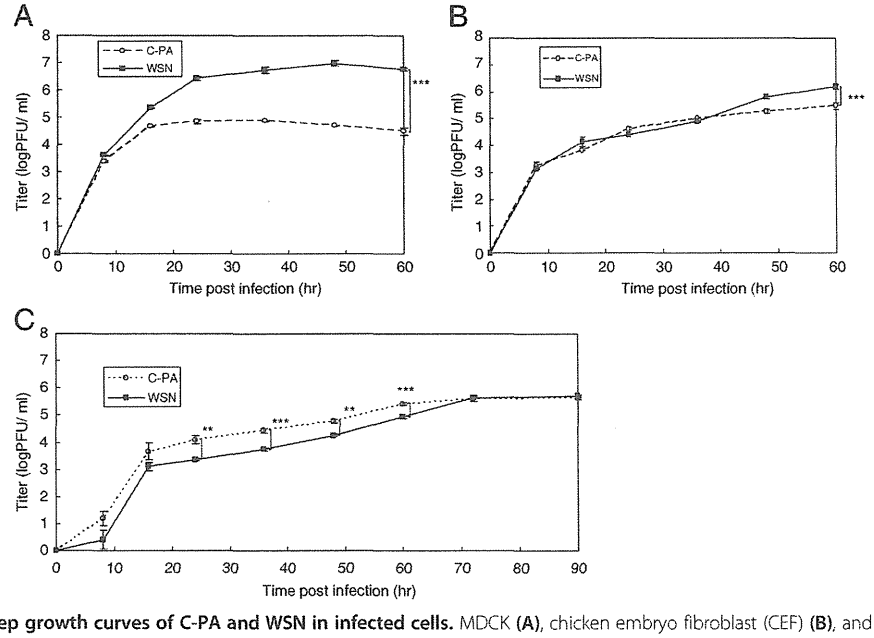

Figure 2 Multi-step growth curves of C-PA and WSN in infected cells. MDCK **(A)**, chicken embryo fibroblast (CEF) **(B)**, and Vero **(C)** cells were infected with C-PA or WSN at a multiplicity of infection (MOI) of 0.01. Viruses were harvested 8, 16, 24, 36, 48, and 60 hr (additional 72 and 90 hr for Vero cells) after infection and their titers on MDCK cells measured by a plaque-formation assay. The mean and standard deviation (error bar in the graph) of each plaque titer were calculated from 3 independent experiments. Statistical significance was evaluated with Student's *t*-test. **$p < 0.01$, ***$p < 0.005$.

No cytopathic effect was apparent in Vero cells (data not shown).

We next compared single-step growth of C-PA and WSN in MDCK and Vero cells (Figure 3). The C-PA titers in both MDCK and Vero cells between 4 and 12 hr pi were higher than those of WSN. The C-PA titer in MDCK cells 12 hr pi ($1.6 \pm 0.9 \times 10^6$ PFU/mL) was significantly higher than that of WSN ($1.3 \pm 0.7 \times 10^5$ PFU/mL) ($p < 0.005$, Figure 3A). The C-PA titer in Vero cells 12 hr pi ($1.6 \pm 0.9 \times 10^5$ PFU/mL) was significantly higher than that of WSN ($2.9 \pm 0.2 \times 10^4$ PFU/mL) ($p < 0.05$, Figure 3B). The growth of C-PA in both MDCK and Vero cells plateaued 6 hr pi. WSN growth in Vero cells plateaued 8 hr pi, while its titer in MDCK cells continued to increase up to 12 hr pi.

Pathogenicity of the C-PA virus in mice

We also examined the pathogenicity of C-PA in mice. The LD_{50} for mouse nasal infection was calculated from the survival rate of the infected mice by the method of Reed and Münch (Figure 4) [43]. The LD_{50} values of C-PA and WSN were 5×10^5 PFU and 1×10^4 PFU, respectively. The pathogenicity of C-PA is therefore lower than that of WSN, despite its higher RdRp activity, both in cell culture (as reflected by the multi-step growth) and in mice.

We thus confirmed the discrepancy between the RdRp activity and pathogenicity both in cells (virus titer) and in mice. The genome sequence of the C-PA stock was confirmed to be identical to that of the genome reconstitution plasmids.

Interferon induction

Because the multi-step growth activity of C-PA was lower than that of WSN in MDCK and CEF cells but better in Vero cells, and because the single-step growth activity of C-PA was better than that of WSN in both MDCK and Vero cells, we examined the effect of C-PA

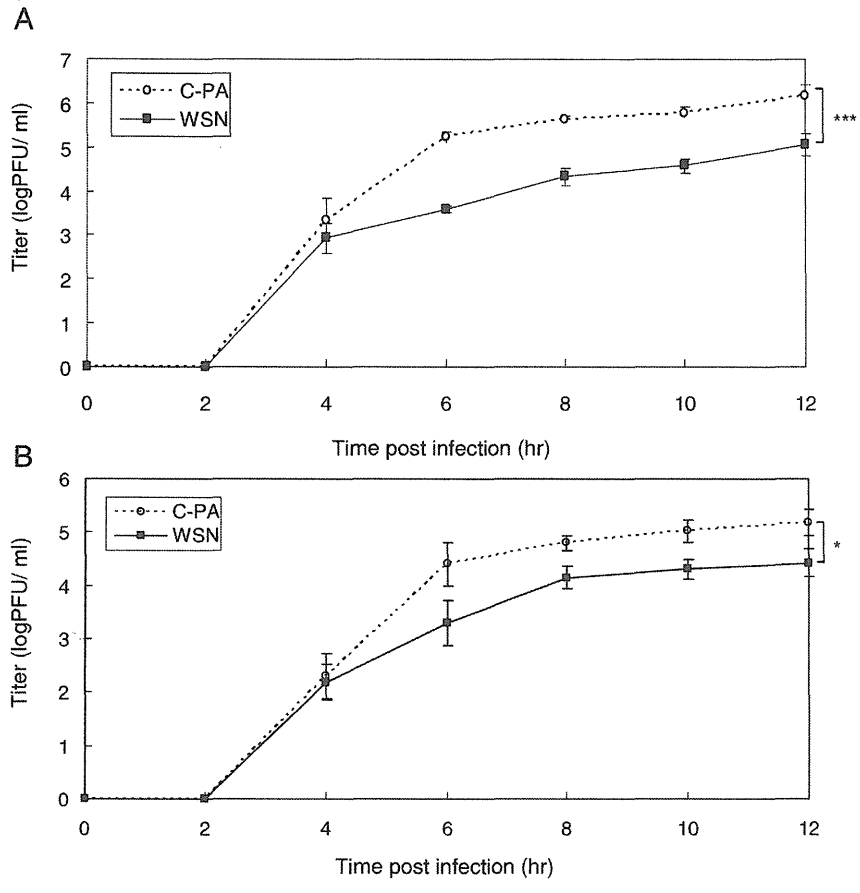

Figure 3 Single-step growth curves of C-PA and WSN in infected cells. MDCK **(A)** and Vero **(B)** cells were infected with C-PA or WSN at an MOI of 5. Viruses were harvested 2, 4, 6, 8, 10, and 12 hr after infection and their titers on MDCK cells measured by a plaque-formation assay. The mean and standard deviation (error bar in the graph) of each plaque titer were calculated from 3 independent experiments. Statistical significance was evaluated with Student's *t*-test. *$p < 0.05$, ***$p < 0.005$.

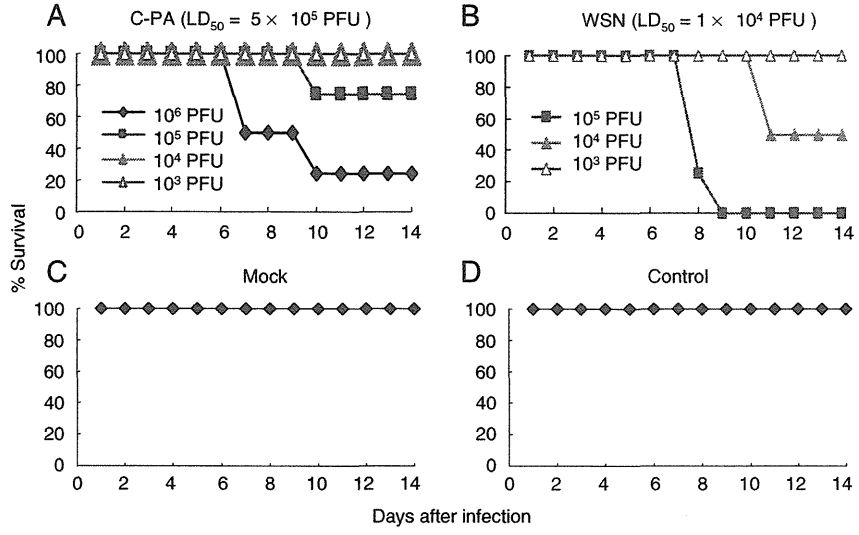

Figure 4 Survival curve of mice infected with C-PA or WSN. Groups of 4 mice were inoculated intra-nasally with 10^6, 10^5, 10^4, or 10^3 plaque-forming units (PFU) of C-PA **(A)** or 10^5, 10^4, or 10^3 PFU of WSN **(B)** in a volume of 50 μL. The survival curves of the mock-infected **(C)** and non-treated (control) **(D)** mice are also shown. Survival status was monitored daily. LD_{50} is indicated above the graph (A and B).

on the activity of the host cellular defense system. First, we examined interferon β induction in 293 T cells by measuring the activity of its promoter (Figure 5). A small amount of interferon β was induced in cells infected with either C-PA or WSN 4 hr pi. However, interferon β promoter activity was almost 3-fold higher ($p < 0.01$) in the C-PA-infected cells than in the WSN-infected cells 8 hr pi.

TUNEL assay

Next, we examined the induction of apoptosis in MDCK cells by performing TUNEL assays hourly from 8 to 16 hr pi and once more 24 hr pi. The numbers of TUNEL-positive cells in 3 random fields were counted (Figure 6A). Before 11 hr pi, we found fewer than 5 TUNEL-positive cells per field in either C-PA- or WSN-infected cells. Then, beginning 12 hr pi, the numbers of the C-PA-infected TUNEL-positive cells increased to 20 ± 3.5 (12 hr), 27 ± 2.5 (13 hr), 41 ± 4.0 (14 hr), 46 ± 2.6 (15 hr), 48 ± 2.6 (16 hr), and 28 ± 3.5 (24 hr). The numbers of the WSN-infected TUNEL-positive cells remained less than 6 until 16 hr and then increased to 40 ± 4.6 at 24 hr pi. From 12 to 16 hr pi, significantly more TUNEL-positive cells were observed among the C-PA-infected cells than among the WSN-infected cells ($p < 0.005$). TUNEL-positive cells were clearly observed among both C-PA- and WSN-infected cells, and significantly more TUNEL-positive cells were observed among WSN-infected cells than among C-PA-infected cells 24 hr pi ($p < 0.05$). In conclusion, TUNEL-positive cells appeared earlier in C-PA-infected cells than in WSN-infected cells. No differences in TUNEL staining were found among cells transfected with WSN and H5N1 Cambodia single-protein-expression plasmids (PB2, PB1, PA, HA, NP, NA, M1, M2, NS1, and NS2) or pcDNA3.1 (data not shown).

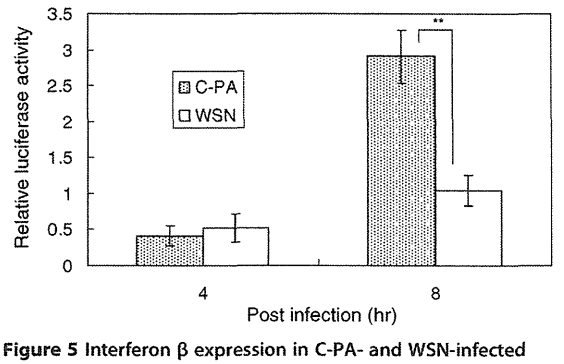

Figure 5 Interferon β expression in C-PA- and WSN-infected cells. Interferon induction levels 4 and 8 hr pi were measured as the luciferase activity from p-125Luc. The mean and standard deviation (error bar) of luciferase activity were calculated from 3 independent measurements. Statistical significance was evaluated with Student's *t*-test. **$p < 0.01$.

Caspase 3, 8, and 9 activities

TUNEL-positive cells may be apoptotic. Caspases are central players in both the intrinsic and the extrinsic pathways of apoptosis [44-46]. We therefore measured the activities of caspases 3, 8, and 9 in C-PA- and WSN-infected cells 10 hr pi, 2 hr before TUNEL-positive cells could first be observed among C-PA-infected cells, in order to confirm

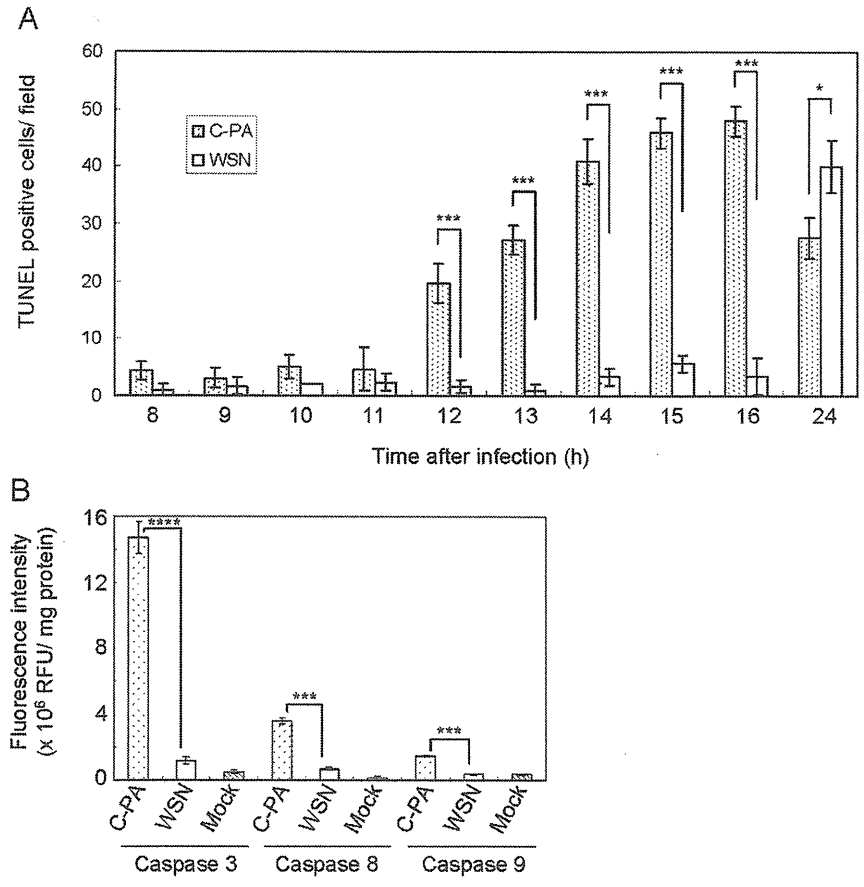

Figure 6 TUNEL staining and Caspase 3, 8, and 9 activities of C-PA- and WSN-infected cells. A. TUNEL assays were performed on C-PA- and WSN-infected MDCK cells at the indicated time after infection. The mean and standard deviation (error bar) of the number of TUNEL-positive cells counted from 3 random fields were calculated. **B.** The activities of caspases 3, 8, and 9 in C-PA- and WSN-infected MDCK cells were measured 10 hr pi. Caspase activity is expressed as the fluorescence intensity/total cellular protein (mg) calculated from 3 independent measurements. Mock: mock-infected MDCK cells. Statistical significance was evaluated with Student's *t*-test. *$p < 0.05$, ***$p < 0.005$, ****$p < 0.0005$.

the induction of apoptosis (Figure 6B). The activities of caspases 3 ($14.7 \pm 9.8 \times 10^6$ RFU/mg protein, $p < 0.0005$), 8 ($3.6 \pm 0.2 \times 10^6$ RFU/mg protein, $p < 0.005$), and 9 ($1.5 \pm 0.5 \times 10^6$ RFU/mg protein, $p < 0.005$) were higher in C-PA-infected cells than in WSN-infected cells 10 hr pi (comparisons evaluated by Student's *t* test). The caspase activities in WSN-infected cells were similar to those in mock-infected cells, indicating that WSN infection did not induce apoptosis 10 hr pi. The activation of caspase 9 in C-PA-infected cells indicates that C-PA infection induces apoptosis through the mitochondrial pathway [47-49], and the apoptosis induction by C-PA began at an early time after infection at which no apoptosis was induced by WSN infection.

Histopathology and TUNEL assay of infected mice

Finally, we compared the pathological changes in the lung between C-PA- and WSN-infected mice. The histopathological appearances were similar (Figure 7). The major difference between C-PA- and WSN-infected lungs is that pulmonary edema around blood vessels was present in the C-PA-infected lungs from day 1 pi, although it was also present in WSN-infected lungs on days 3 and 4 pi. On the first day of infection, a moderate amount of lymphocyte infiltration was observed around the bronchioles of C-PA-infected mouse lungs, and this inflammation decreased on days 3 and 4. More lymphocyte infiltration around the bronchioles was observed in WSN-infected mouse lungs on days 1–3, with the most severe inflammation on day 2, and only mild inflammation was observed on day 4. No pathological change was observed in the mock-infected or non-infected mouse lungs.

We simultaneously analyzed these samples by TUNEL assay. A few TUNEL-positive cells were observed in both C-PA- and WSN-infected mouse lungs on days 1–4 pi,

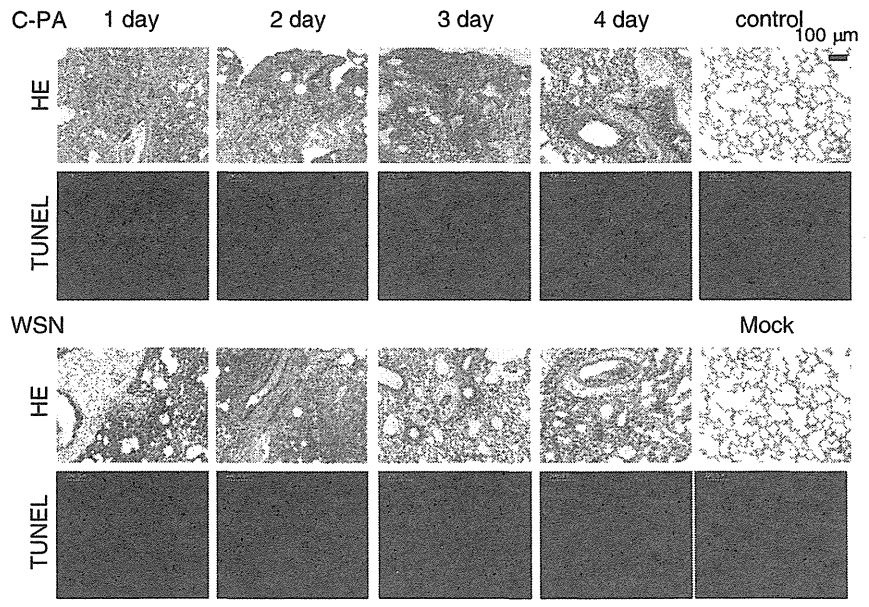

Figure 7 Histopathology of C-PA- and WSN-infected mouse lungs. The lungs of mice infected with C-PA or WSN (10^5 PFU/mouse) at the indicated days after infection were imaged after hematoxylin and eosin (HE) or TUNEL staining. Control: non-infected mouse lung. The bar above the picture indicates 100 μm and the bars in the fluorescence microgram indicate 200 μm.

but the numbers did not clearly differ between the 2 viruses. The histopathological findings indicated recovery of the C-PA-infected mouse lungs, which is consistent with the lower pathogenicity of C-PA.

Discussion

The activation of replicon activity by H5N1 HPAIV PA observed in this study has been reported several times (Figure 1) [34,50,51]. Influenza viruses with high polymerase activity have been reported to show high pathogenicity [7,8]. Therefore, reassortment of H5N1 HPAIV PA into human influenza viruses, including the seasonal influenza viruses (H1N1 and H3N2) and the pandemic influenza virus (H1N1), is a serious concern [34], although this event may not occur easily [32]. The major factor for host adaptation in H5N1 HPAIV RNP is PB2, which shows a strong correlation with pathogenicity in mammalian hosts, including humans [30,31,51-55].

The WSN reconstitution system [56] was used to analyze the effect of H5N1 Cambodia PA in an animal influenza virus (H1N1). Contrary to our expectation, the multi-step growth of C-PA in MDCK and CEF cells was less than that of WSN, and its pathogenicity was low because of this attenuation (Figures 2, 4). We confirmed the absence of mutations in the C-PA genome. As we previously found a similar discrepancy in influenza promoter/origin function due to a difference in activation of the host defense system [42], we examined whether the discrepancy between RdRp activity and pathogenicity was also due to differences in host defense. As the multi-step growth of C-PA in Vero cells was better than that of WSN, and because its single-step growth, which is highly dependent on the polymerase activity, in both MDCK and Vero cells was better than that of WSN (Figure 3), we first examined the activity of the interferon β promoter and found that it was strongly activated (Figure 5) in CPA-infected cells.

Type I interferon is induced in virus-infected cells by a signal transduction pathway beginning with retinoic-acid-inducible gene-I (RIG-I), which recognizes 5′-triphosphate-containing influenza RNA [57-62]. In C-PA-infected cells, a large amount of vRNA was expressed from early stages of infection, which might more strongly trigger interferon induction (Figures 5 and Additional file: Figure S3) and thereby induce an antiviral state in uninfected cells that protected them from influenza infection (Additional file: Figure S2A) [63-65]. The better multi-step growth of C-PA relative to WSN in Vero cells, which are defective in type-I interferon production [66] (Figure 2C), and the better single-step growth of C-PA than of WSN (Figure 3), are consistent with the high *in vitro* polymerase activity and strong interferon induction in C-PA infected cells.

Apoptosis (programmed cell death) is another mechanism by which cells restrict viral infection including influenza [67]. However, virus-induced apoptosis causes tissue damage, which is one of the mechanisms of influenza pathogenicity [68]. Apoptosis also aids in the

release of influenza viruses [69,70]. WSN induced apoptosis in MDCK cells late in infection [71]. However, no apoptosis was induced by expression of any single protein of either WSN or H5N1 Cambodia. Apoptosis was strongly induced in C-PA-infected cells beginning early in infection when no apoptosis was induced in WSN-infected cells (Figure 6). The activation of caspase 9 indicated that this apoptosis was mediated through the mitochondrial pathway [72]. The increased expression of vRNA (Additional file: Figure S3) in C-PA infected cells due to the high replication activity promoted by H5N1 PA (Figure 1) induced both interferon and apoptosis, resulting in attenuation of C-PA proliferation (Figure 2). Neither caspase 3 nor 8 was induced by expression of WSN PA or Cambodia PA alone (data not shown). The strong induction of interferon discussed above also stimulates the induction of apoptosis *via* RNA-dependent protein kinase (PKR) [73]. Such rapid induction of apoptosis was also observed in duck cells infected with HPAIV [68]. However, in case of C-PA, early induction of apoptosis attenuated the proliferation of the virus and thus decreased its pathogenicity.

PB1-F2 is the only influenza virus protein that induces apoptosis in infected monocytes and potentiates apoptosis during infection [74-76]. The WSN PB1-F2 proteins of WSN and C-PA are identical. Kinetic analysis of viral RNAs (Additional file: Figure S3) indicates that PB1-F2 is unlikely to contribute to the strong induction of apoptosis in C-PA infected cells.

C-PA infection strongly induced both interferon production and apoptosis early in infection, which attenuated virus proliferation and pathogenicity despite high RdRp activity. This may be another reason, in addition to poor adaptation, for the difficulty of obtaining reassortant viruses carrying H5N1 HPAIV PA [31,32].

Methods

Cell culture

293 T and Vero cells were maintained in Dulbecco's modified Eagle minimal essential medium (DMEM) containing 10% fetal bovine serum (FBS). CEFs were prepared from 11-day-old embryonated chicken eggs by trypsin digestion and stored in liquid nitrogen. CEF and MDCK cells were maintained in DMEM containing 10% or 5% FBS, respectively.

Replicon assay

A standard replicon assay was performed as previously described [41,42,77]. Luciferase activity was measured using the Dual-Glo luciferase assay kit and a GloMax 96 Microplate Luminometer (Promega, Fitchburg, USA) after transfection of 0.1 μg each of pCPB2, pCPB1, pCPA, pCNP, and ppolINSluc and 0.01 μg of pRL_{SV40} (Promega) using Lipofectamine 2000 (Invitrogen, Carlsbad, USA). The PB2, PB1, PA, and NP genes of influenza A/Cambodia/P096/2005 (H5N1) [40] and A/WSN/33 (H1N1) [56] were PCR-amplified using specific oligonucleotides and cloned into pcDNA3.1(+) (Invitrogen), resulting in pcCamPB2wt, pcCamPB1, pcCamPA, pcCamNP, pcWSNPB2, pcWSNPB1, pcWSNPA, and pcWSNNP, respectively. Only data in which the variation of the Renilla luciferase activity was less than 3-fold variations were used. The oligonucleotide sequence information will be made available upon request.

Expression, purification, and *in vitro* transcription of the influenza virus RdRp

Expression, purification, and *in vitro* transcription of the influenza virus RdRp were performed as previously described [42,77,78]. Briefly, 100 nM influenza RdRp was incubated in 50 mM Tris–HCl (pH 8.0), 8 mM $MgCl_2$, 150 mM NaCl, 2 mM DTT, 0.5 mM ATP, 0.5 mM CTP, 0.5 mM GTP, 0.05 mM [α-^{32}P] UTP, 0.1 mM ApG or 0.01 mg/mL globin mRNA, 2000 U/mL RNase inhibitor, and 200 nM v84 and c84 model template RNA at 25 °C for 90 min. The product was analyzed by PAGE on 6% gels containing 8 M urea and the images analyzed with a Typhoon Trio plus (GE Healthcare, Bucks, UK).

Model RNA templates

v84 and c84 model RNA templates were prepared as previously reported [11].

Western blotting

Proteins were blotted onto nitrocellulose membranes (Millipore, Billerica, USA) by semi-dry electroblotting (Bio-Rad, Hercules, USA) after SDS-PAGE on 10% gels. The blotted membranes were blocked with 10% skim milk in 20 mM Tris–HCl (pH 7.5), 150 mM NaCl, and 0.02% Tween 20 (TBST), and western blotting was performed using rabbit anti-PB1, -PB2, -PA [11], and -PR8 (1:1,000 each) and anti-actin (1:100) antibodies as the primary antibodies. The membranes were then incubated with alkaline phosphatase-conjugated anti-rabbit IgG (1:7,500) or anti-mouse IgG (1:7,500), and the positions of the bound antibodies were visualized with nitro-blue tetrazolium (NBT) and 5-bromo-4-chloro-3-indolyl phosphate (BCIP).

Reconstitution of influenza virus and plaque-formation assay

pHH21 and the influenza virus 12-plasmid reconstitution system of WSN were kindly provided by Dr. Hobom and Dr. Kawaoka [56]. The H5N1 A/Cambodia/P0322095/2005 [40] PA sequence was inserted into ppolI-WSN-PA, resulting in ppolI-Cam-PA. The influenza virus WSN strain (WSN) and WSN carrying H5N1

Cambodia PA (C-PA) were reconstituted by co-transfection of 293 T cells with ppolI-WSN-PB2, ppolI-WSN-PB1, ppolI-WSN-PA or ppolI-Cam-PA, ppolI-WSN-HA, ppolI-WSN-NP, ppolI-WSN-NA, ppolI-WSN-M, and ppolI-WSN-NS with pCPB2, pCPB1, pCPA, and pCNP [10,56] using Lipofectamine 2000. The reconstituted viruses were recovered from the culture media 72 hr post-transfection. The viruses were plaque-purified, amplified, and titered on MDCK cells by a plaque-formation assay and stored at −80 °C. The genome sequences of all viruses were determined by RT-PCR. The primer sequences used will be made available upon request.

Virus growth assay

MDCK, CEF, and Vero cells in 3.5-cm dishes (21 dishes of MDCK cells and CEFs, 27 dishes of Vero cells per a virus) were infected with WSN and C-PA at an MOI of 0.01 at 37 °C for 1 hr (multi-step growth assay). The cells were washed 3× with phosphate-buffered saline (PBS) and incubated with 2 mL of DMEM containing 2% FBS (without trypsin) at 37 °C, as WSN replicates without trypsin [79]. All of the supernatants of 3 dishes of each cell were taken 6, 12, 24, 36, 48, and 60 hr (and also at 72 and 90 hr for Vero cells) after infection and stored at −80 °C. Virus growth was also tested in MDCK and Vero cells after infection at an MOI of 5 (single-step growth assay). Supernatants were harvested 2, 4, 6, 8, 10, and 12 hr after infection. The viruses in the supernatants were titered on MDCK cells by a plaque-formation assay.

Mouse infection

Groups of 4 6-week-old female BALB/c mice (Sino-British Laboratory Animal, Shanghai, China) were anesthetized with ether and inoculated with 10^5, 10^4, or 10^3 PFU of WSN or 10^6, 10^5, 10^4, or 10^3 PFU of C-PA in a volume of 50 μL by nasal dropping. Four mice were inoculated with 50 μL of PBS as a mock-infection control. The survival rates were monitored daily and the 50% lethal doses (LD_{50}s) calculated [41].

Histopathological analysis

Six-week-old female BALB/c mice were anesthetized with ether and inoculated with 10^5 PFU of WSN or C-PA in 50 μL by nasal dropping. Mice were inoculated with 50 μL of PBS as a mock-infection control. A non-treated mouse was used as a non-treated control. The mock-infected and infected mice were sacrificed by cervical dislocation under anesthesia on days 1, 2, 3, and 4 after infection, and their lungs were removed and fixed with 3.5% formalin/PBS at 25 °C for 2 days. The lungs were embedded in paraffin blocks, sectioned at 4-μm thickness, and stained with hematoxylin and eosin (HE).

TUNEL assay

Cells were placed on cover slips in 24-well plates and infected with WSN or C-PA at an MOI of 0.01. Eight, 9, 10, 11, 12, 13, 14, 15, 16, and 24 hr after infection, cells were fixed with 1% formalin/PBS. The TUNEL assay was performed using the DeadEnd™ Fluorometric TUNEL system according to the company's instructions. The samples were observed using a fluorescence microscope (Leica DM IRB, Leica, Wetzlar, Germany), and the numbers of TUNEL positive cells in 3 random fields were counted.

Caspase activity

MDCK cells were plated in 10-cm-diameter plates and infected with WSN or C-PA at an MOI of 0.01. 10 hr after infection, the cells were harvested and the activities of caspases 3, 8, and 9 measured using the Caspase-3/CPP32 Fluorometric Assay kit, the Caspase 8/FLICE Fluorometric Assay kit, and the Caspase 9 Fluorometric Assay kit (Biovision, Inc., Milpitas, USA) according to the manufacturer's instructions.

Interferon induction

Interferon induction was analyzed by measuring the luciferase activity of cells transfected with p-125Luc, which was kindly provided by Dr. Fujita [80]. 293 T cells were transfected with p-125Luc (1 μg) and pRL_{SV40} (100 ng). Four hours post-transfection, the cells were infected with WSN or C-PA at an MOI of 0.01. The interferon promoter activity was measured as the luciferase activity using the Dual-Glo luciferase assay kit and a GloMax 96 Microplate Luminometer (Promega) and normalized as the firefly luciferase/Renilla luciferase activity ratio.

Chemicals and radioisotopes

Non-radiolabeled nucleotides were purchased from GE Healthcare, [α-^{32}P]UTP from New England Nuclear (PerkinElmer Life Sciences, Waltham, USA), and T7 RNA polymerase, T4 nucleotide kinase, oligonucleotides, human placental RNase inhibitor, and restriction enzymes from Takara (Dalian, China). The RPAIII Ribonuclease Protection Assay Kit was purchased from Ambion (Austin, USA). Anti-actin antibodies were purchased from Sigma Aldrich (St. Louis, USA). The Dual-Glo luciferase assay kit, DeadEnd™ Fluorometric TUNEL system, alkaline phosphatase-conjugated anti-rabbit and anti-mouse IgG's, NBT, and BCIP were purchased from Promega. DMEM, FBS, Lipofectamine 2000, and Trizol reagent were purchased from Invitrogen.

Statistical analysis

The statistical significance levels of the data were evaluated by Student's *t*-test, with $p < 0.05$ indicating statistical significance.

Additional file

Additional file 1: Results, Methods. Figure S1. Expression of RdRp subunits and NP in the transfected cells. **Figure S2.** Time course of NP protein expression by C-PA and WSN. **Figure S3.** Time courses of NP vRNA, cRNA, and mRNA expression by C-PA and WSN.

Competing Interests

The authors declare that they have no competing interests.

Author's contributions

QW, SZ, HJ, JW, LW, YM, and KX carried out the experiments. SS, FY, and MK analyzed caspase activity and mouse lung tissues. PB and VD isolated and cloned HPAIV H5N1 Cambodia. QW, SZ, SB, and TT conceived of the study. QW and SZ analyzed the data and drafted the manuscript, and SB and TT reviewed the manuscript. All authors read and approved the final manuscript.

Acknowledgements

We thank Drs. T. Fujita, G. Hobom, and Y. Kawaoka for p-125Luc, pHH21, and the influenza virus 12-plasmid reconstitution system, respectively. This work was supported by Grants-in-aid from the Chinese Academy of Sciences (0514P51131), the National Science Foundation of China (30970153), the Li Ka Shing Foundation (0682P11131), RESPARI (0581P14131), and European Union (FLUINNATE 0681P21131).

Author details

[1]Units of Molecular Virology, the Key Laboratory of Molecular Virology & Immunology, Institut Pasteur of Shanghai, Chinese Academy of Sciences, 411 Hefei Road, 200025, Shanghai, P. R. China. [2]Units of Viral Genome Regulation, the Key Laboratory of Molecular Virology & Immunology, Institut Pasteur of Shanghai, Chinese Academy of Sciences, 411 Hefei Road, 200025, Shanghai, P. R. China. [3]Shanghai Medical College of Fudan University, Yixueyuan Road 138, Shanghai 200032, P. R. China. [4]Roche R&D Center China LTD, 720 Cai Lun Road, Building 5, Pudong, Shanghai 201203, P. R. China. [5]Department of Microbiology and Cell Biology, Tokyo Metropolitan Institute of Medical Biology, 3-18-22 Honkomagome, Bunkyo-Ku, Tokyo 113-8613, Japan. [6]Institut Pasteur in Cambodia, 5 Monivong Blvd, P.O. Box 983, Phnom Penh, Cambodia. [7]Choju Medical Institute, Fukushimura Hospital, 19-14 Azanakayama, Noyori-cho, Toyohashi, Aichi 441-8124, Japan.

Received: 14 October 2011 Accepted: 21 May 2012
Published: 8 June 2012

References

1. Webster RG, Sharp GB, Claas EC: **Interspecies transmission of influenza viruses.** *Am J Respir Crit Care Med* 1995, **152**:S25–30.
2. Kawaoka Y, Krauss S, Webster RG: **Avian-to-human transmission of the PB1 gene of influenza A viruses in the 1957 and 1968 pandemics.** *J Virol* 1989, **63**:4603–4608.
3. Lindstrom SE, Cox NJ, Klimov A: **Genetic analysis of human H2N2 and early H3N2 influenza viruses, 1957–1972: evidence for genetic divergence and multiple reassortment events.** *Virology* 2004, **328**:101–119.
4. Dawood FS, Jain S, Finelli L, Shaw MW, Lindstrom S, Garten RJ, Gubareva LV, Xu X, Bridges CB, Uyeki TM: **Emergence of a novel swine-origin influenza A (H1N1) virus in humans.** *N Engl J Med* 2009, **360**:2605–2615.
5. Wasilenko JL, Lee CW, Sarmento L, Spackman E, Kapczynski DR, Suarez DL, Pantin-Jackwood MJ: **NP, PB1, and PB2 viral genes contribute to altered replication of H5N1 avian influenza viruses in chickens.** *J Virol* 2008, **82**:4544–4553.
6. Hulse-Post DJ, Franks J, Boyd K, Salomon R, Hoffmann E, Yen HL, Webby RJ, Walker D, Nguyen TD, Webster RG: **Molecular changes in the polymerase genes (PA and PB1) associated with high pathogenicity of H5N1 influenza virus in mallard ducks.** *J Virol* 2007, **81**:8515–8524.
7. Seyer R, Hrincius ER, Ritzel D, Abt M, Mellmann A, Marjuki H, Kuhn J, Wolff T, Ludwig S, Ehrhardt C: **Synergistic adaptive mutations in the hemagglutinin and polymerase acidic protein lead to increased virulence of pandemic 2009 H1N1 influenza A virus in mice.** *J Infect Dis* 2012, **205**:262–271.
8. Salomon R, Franks J, Govorkova EA, Ilyushina NA, Yen HL, Hulse-Post DJ, Humberd J, Trichet M, Rehg JE, Webby RJ, *et al*: **The polymerase complex genes contribute to the high virulence of the human H5N1 influenza virus isolate A/Vietnam/1203/04.** *J Exp Med* 2006, **203**:689–697.
9. Palese P, Shaw ML: **Orthomyxoviridae: The Viruses and Their Replication.** In *Fields Virology*. 5th edition. Edited by Knipe DM, Howley PM. Philadelphia: Lippincott Williams & Wilkins; 2007:1647–1689.
10. Toyoda T, Adyshev DM, Kobayashi M, Iwata A, Ishihama A: **Molecular assembly of the influenza virus RNA polymerase: determination of the subunit-subunit contact sites.** *J Gen Virol* 1996, **77**(Pt 9):2149–2157.
11. Kobayashi M, Toyoda T, Ishihama A: **Influenza virus PB1 protein is the minimal and essential subunit of RNA polymerase.** *Arch Virol* 1996, **141**:525–539.
12. Biswas SK, Nayak DP: **Mutational analysis of the conserved motifs of influenza A virus polymerase basic protein 1.** *J Virol* 1994, **68**:1819–1826.
13. Ulmanen I, Broni BA, Krug RM: **Role of two of the influenza virus core P proteins in recognizing cap 1 structures (m7G pppNm) on RNAs and in initiating viral RNA transcription.** *Proc Natl Acad Sci U S A* 1981, **78**:7355–7359.
14. Li ML, Rao P, Krug RM: **The active sites of the influenza cap-dependent endonuclease are on different polymerase subunits.** *EMBO J* 2001, **20**:2078–2086.
15. Blaas D, Patzelt E, Kuechler E: **Cap-recognizing protein of influenza virus.** *Virology* 1982, **116**:339–348.
16. Crepin T, Dias A, Palencia A, Swale C, Cusack S, Ruigrok RW: **Mutational and metal binding analysis of the endonuclease domain of the influenza virus polymerase PA subunit.** *J Virol* 2010, **84**:9096–9104.
17. Dias A, Bouvier D, Crepin T, McCarthy AA, Hart DJ, Baudin F, Cusack S, Ruigrok RW: **The cap-snatching endonuclease of influenza virus polymerase resides in the PA subunit.** *Nature* 2009, **458**:914–918.
18. Fodor E, Brownlee G: **Influenza virus replication.** In *Influenza*. Edited by Potter C. Amsterdam: Elsevier; 2002:1–29.
19. Hara K, Schmidt FI, Crow M, Brownlee GG: **Amino acid residues in the N-terminal region of the PA subunit of influenza A virus RNA polymerase play a critical role in protein stability, endonuclease activity, cap binding, and virion RNA promoter binding.** *J Virol* 2006, **80**:7789–7798.
20. Yuan P, Bartlam M, Lou Z, Chen S, Zhou J, He X, Lv Z, Ge R, Li X, Deng T, *et al*: **Crystal structure of an avian influenza polymerase PA(N) reveals an endonuclease active site.** *Nature* 2009, **458**:909–913.
21. Kawakami K, Mizumoto K, Ishihama A: **RNA polymerase of influenza virus. IV. Catalytic properties of the capped RNA endonuclease associated with the RNA polymerase.** *Nucleic Acids Res* 1983, **11**:3637–3649.
22. Plotch SJ, Bouloy M, Ulmanen I, Krug RM: **A unique cap(m7G pppXm)-dependent influenza virion endonuclease cleaves capped RNAs to generate the primers that initiate viral RNA transcription.** *Cell* 1981, **23**:847–858.
23. Krug RM, Alonso-Caplan FV, Julkunen I, Katze MG: **Expression and replication of the influenza virus genome.** In Edited by Krug RM. New York: Plenum Press; 1989:89–152.
24. Deng T, Vreede FT, Brownlee GG: **Different de novo initiation strategies are used by influenza virus RNA polymerase on its cRNA and viral RNA promoters during viral RNA replication.** *J Virol* 2006, **80**:2337–2348.
25. Zhang S, Wang J, Wang Q, Toyoda T: **Internal initiation of influenza virus replication of v- and cRNA in vitro.** *J Biol Chem* 2010, **285**:41194–41201.
26. Neumann G, Shinya K, Kawaoka Y: **Molecular pathogenesis of H5N1 influenza virus infections.** *Antivir Ther* 2007, **12**:617–626.
27. Abdel-Ghafar AN, Chotpitayasunondh T, Gao Z, Hayden FG, Nguyen DH, de Jong MD, Naghdaliyev A, Peiris JS, Shindo N, Soeroso S, Uyeki TM: **Update on avian influenza A (H5N1) virus infection in humans.** *N Engl J Med* 2008, **358**:261–273.
28. Uyeki TM: **Global epidemiology of human infections with highly pathogenic avian influenza A (H5N1) viruses.** *Respirology* 2008, **13** (Suppl 1):S2–9.
29. Maines TR, Chen LM, Matsuoka Y, Chen H, Rowe T, Ortin J, Falcon A, Nguyen TH, le Mai Q, Sedyaningsih ER, *et al*: **Lack of transmission of H5N1 avian-human reassortant influenza viruses in a ferret model.** *Proc Natl Acad Sci U S A* 2006, **103**:12121–12126.
30. Li C, Hatta M, Watanabe S, Neumann G, Kawaoka Y: **Compatibility among polymerase subunit proteins is a restricting factor in reassortment between equine H7N7 and human H3N2 influenza viruses.** *J Virol* 2008, **82**:11880–11888.

31. Chen LM, Davis CT, Zhou H, Cox NJ, Donis RO: **Genetic compatibility and virulence of reassortants derived from contemporary avian H5N1 and human H3N2 influenza A viruses.** *PLoS Pathog* 2008, 4:e1000072.
32. Hatta M, Halfmann P, Wells K, Kawaoka Y: **Human influenza a viral genes responsible for the restriction of its replication in duck intestine.** *Virology* 2002, **295**:250–255.
33. Gutiérrez R, Naughtin M, Horm S, San S, Buchy P: **A(H5N1) Virus Evolution in South East Asia.** *Viruses* 2009, **1**:335–361.
34. Kashiwagi T, Leung BW, Deng T, Chen H, Brownlee GG: **The N-terminal region of the PA subunit of the RNA polymerase of influenza A/HongKong/156/97 (H5N1) influences promoter binding.** *PLoS One* 2009, 4:e5473.
35. Fodor E, Crow M, Mingay LJ, Deng T, Sharps J, Fechter P, Brownlee GG: **A single amino acid mutation in the PA subunit of the influenza virus RNA polymerase inhibits endonucleolytic cleavage of capped RNAs.** *J Virol* 2002, **76**:8989–9001.
36. Hara K, Shiota M, Kido H, Ohtsu Y, Kashiwagi T, Iwahashi J, Hamada N, Mizoue K, Tsumura N, Kato H, Toyoda T: **Influenza virus RNA polymerase PA subunit is a novel serine protease with Ser624 at the active site.** *Genes Cells* 2001, **6**:87–97.
37. Sanz-Ezquerro JJ, Zurcher T, de la Luna S, Ortin J, Nieto A: **The amino-terminal one-third of the influenza virus PA protein is responsible for the induction of proteolysis.** *J Virol* 1996, **70**:1905–1911.
38. Song MS, Pascua PN, Lee JH, Baek YH, Lee OJ, Kim CJ, Kim H, Webby RJ, Webster RG, Choi YK: **The polymerase acidic protein gene of influenza a virus contributes to pathogenicity in a mouse model.** *J Virol* 2009, **83**:12325–12335.
39. Kashiwagi T, Hara K, Nakazono Y, Hamada N, Watanabe H: **Artificial hybrids of influenza A virus RNA polymerase reveal PA subunit modulates its thermal sensitivity.** *PLoS One* 2010, 5:e15140.
40. Buchy P, Mardy S, Vong S, Toyoda T, Aubin JT, Miller M, Touch S, Sovann L, Dufourcq JB, Richner B, *et al*: **Influenza A/H5N1 virus infection in humans in Cambodia.** *J Clin Virol* 2007, **39**:164–168.
41. Toyoda T, Hara K, Imamura Y: **Ser624 of the PA subunit of influenza A virus is not essential for viral growth in cells and mice, but required for the maximal viral growth.** *Arch Virol* 2003, **148**:1687–1696.
42. Jiang H, Zhang S, Wang Q, Wang J, Geng L, Toyoda T: **Influenza virus genome C4 promoter/origin attenuates its transcription and replication activity by the low polymerase recognition activity.** *Virology* 2010, **408**:190–196.
43. Reed LJ, Muench H: **Simple method of estimating 50 per cent endpoinds.** *Amer J Hyg* 1938, **27**:493–497.
44. Wang C, Youle RJ: **The role of mitochondria in apoptosis*.** *Annu Rev Genet* 2009, **43**:95–118.
45. Li J, Yuan J: **Caspases in apoptosis and beyond.** *Oncogene* 2008, **27**:6194–6206.
46. Roulston A, Marcellus RC, Branton PE: **Viruses and apoptosis.** *Annu Rev Microbiol* 1999, **53**:577–628.
47. Desagher S, Martinou JC: **Mitochondria as the central control point of apoptosis.** *Trends Cell Biol* 2000, **10**:369–377.
48. Kroemer G: **The proto-oncogene Bcl-2 and its role in regulating apoptosis.** *Nat Med* 1997, **3**:614–620.
49. Kroemer G: **Mitochondrial implication in apoptosis. Towards an endosymbiont hypothesis of apoptosis evolution.** *Cell Death Differ* 1997, **4**:443–456.
50. Gabriel G, Dauber B, Wolff T, Planz O, Klenk HD, Stech J: **The viral polymerase mediates adaptation of an avian influenza virus to a mammalian host.** *Proc Natl Acad Sci U S A* 2005, **102**:18590–18595.
51. Li Z, Chen H, Jiao P, Deng G, Tian G, Li Y, Hoffmann E, Webster RG, Matsuoka Y, Yu K: **Molecular basis of replication of duck H5N1 influenza viruses in a mammalian mouse model.** *J Virol* 2005, **79**:12058–12064.
52. Hatta M, Gao P, Halfmann P, Kawaoka Y: **Molecular basis for high virulence of Hong Kong H5N1 influenza A viruses.** *Science* 2001, **293**:1840–1842.
53. Gabriel G, Herwig A, Klenk HD: **Interaction of polymerase subunit PB2 and NP with importin alpha1 is a determinant of host range of influenza A virus.** *PLoS Pathog* 2008, 4:e11.
54. Mehle A, Doudna JA: **An inhibitory activity in human cells restricts the function of an avian-like influenza virus polymerase.** *Cell Host Microbe* 2008, **4**:111–122.
55. Mehle A, Doudna JA: **Adaptive strategies of the influenza virus polymerase for replication in humans.** *Proc Natl Acad Sci U S A* 2009, **106**:21312–21316.
56. Neumann G, Watanabe T, Ito H, Watanabe S, Goto H, Gao P, Hughes M, Perez DR, Donis R, Hoffmann E, *et al*: **Generation of influenza A viruses entirely from cloned cDNAs.** *Proc Natl Acad Sci U S A* 1999, **96**:9345–9350.
57. Sarmento L, Afonso CL, Estevez C, Wasilenko J, Pantin-Jackwood M: **Differential host gene expression in cells infected with highly pathogenic H5N1 avian influenza viruses.** *Vet Immunol Immunopathol* 2008, **125**:291–302.
58. Vester D, Rapp E, Gade D, Genzel Y, Reichl U: **Quantitative analysis of cellular proteome alterations in human influenza A virus-infected mammalian cell lines.** *Proteomics* 2009, **9**:3316–3327.
59. Kato H, Takeuchi O, Sato S, Yoneyama M, Yamamoto M, Matsui K, Uematsu S, Jung A, Kawai T, Ishii KJ, *et al*: **Differential roles of MDA5 and RIG-I helicases in the recognition of RNA viruses.** *Nature* 2006, **441**:101–105.
60. Loo YM, Fornek J, Crochet N, Bajwa G, Perwitasari O, Martinez-Sobrido L, Akira S, Gill MA, Garcia-Sastre A, Katze MG, Gale M Jr: **Distinct RIG-I and MDA5 signaling by RNA viruses in innate immunity.** *J Virol* 2008, **82**:335–345.
61. Yoneyama M, Fujita T: **RNA recognition and signal transduction by RIG-I-like receptors.** *Immunol Rev* 2009, **227**:54–65.
62. Rehwinkel J, Tan CP, Goubau D, Schulz O, Pichlmair A, Bier K, Robb N, Vreede F, Barclay W, Fodor E, Reis e Sousa C: **RIG-I detects viral genomic RNA during negative-strand RNA virus infection.** *Cell* 2010, **140**:397–408.
63. Haller O, Kochs G, Weber F: **The interferon response circuit: induction and suppression by pathogenic viruses.** *Virology* 2006, **344**:119–130.
64. Taniguchi T, Takaoka A: **The interferon-alpha/beta system in antiviral responses: a multimodal machinery of gene regulation by the IRF family of transcription factors.** *Curr Opin Immunol* 2002, **14**:111–116.
65. Price GE, Gaszewska-Mastarlarz A, Moskophidis D: **The role of alpha/beta and gamma interferons in development of immunity to influenza A virus in mice.** *J Virol* 2000, **74**:3996–4003.
66. Mosca JD, Pitha PM: **Transcriptional and posttranscriptional regulation of exogenous human beta interferon gene in simian cells defective in interferon synthesis.** *Mol Cell Biol* 1986, **6**:2279–2283.
67. Kuchipudi SV, Dunham SP, Nelli R, White GA, Coward VJ, Slomka MJ, Brown IH, Chang KC: **Rapid death of duck cells infected with influenza: a potential mechanism for host resistance to H5N1.** *Immunol Cell Biol* 2011.
68. Brydon EW, Morris SJ, Sweet C: **Role of apoptosis and cytokines in influenza virus morbidity.** *FEMS Microbiol Rev* 2005, **29**:837–850.
69. Olsen CW, Kehren JC, Dybdahl-Sissoko NR, Hinshaw VS: **bcl-2 alters influenza virus yield, spread, and hemagglutinin glycosylation.** *J Virol* 1996, **70**:663–666.
70. Wurzer WJ, Planz O, Ehrhardt C, Giner M, Silberzahn T, Pleschka S, Ludwig S: **Caspase 3 activation is essential for efficient influenza virus propagation.** *EMBO J* 2003, **22**:2717–2728.
71. McLean JE, Datan E, Matassov D, Zakeri ZF: **Lack of Bax prevents influenza A virus-induced apoptosis and causes diminished viral replication.** *J Virol* 2009, **83**:8233–8246.
72. Machida K, Tsukiyama-Kohara K, Seike E, Tone S, Shibasaki F, Shimizu M, Takahashi H, Hayashi Y, Funata N, Taya C, *et al*: **Inhibition of cytochrome c release in Fas-mediated signaling pathway in transgenic mice induced to express hepatitis C viral proteins.** *J Biol Chem* 2001, **276**:12140–12146.
73. Pe'ery T, Mathews M: **Viral translational strategies and host defense mechanism.** In *Translational Control of Gene Expression*. Edited by Sonenberg N, Hershey J, Mathews M. Cold Spring Harbor: Cold Spring Harbor Laboratory Press; 2000:371–424.
74. McLean JE, Ruck A, Shirazian A, Pooyaei-Mehr F, Zakeri ZF: **Viral manipulation of cell death.** *Curr Pharm Des* 2008, **14**:198–220.
75. Zamarin D, Garcia-Sastre A, Xiao X, Wang R, Palese P: **Influenza virus PB1-F2 protein induces cell death through mitochondrial ANT3 and VDAC1.** *PLoS Pathog* 2005, 1:e4.
76. Zamarin D, Ortigoza MB, Palese P: **Influenza A virus PB1-F2 protein contributes to viral pathogenesis in mice.** *J Virol* 2006, **80**:7976–7983.
77. Zhang S, Wang Q, Wang J, Mizumoto K, Toyoda T: **Two mutations in the C-terminal domain of influenza virus RNA polymerase PB2 enhance transcription by enhancing cap-1 RNA binding activity.** *Biochim Biophys Acta* 2012, **1819**:78–83.
78. Zhang S, Weng L, Geng L, Wang J, Zhou J, Deubel V, Buchy P, Toyoda T: **Biochemical and kinetic analysis of the influenza virus RNA polymerase purified from insect cells.** *Biochem Biophys Res Commun* 2010, **391**:570–574.

79. Goto H, Wells K, Takada A, Kawaoka Y: **Plasminogen-binding activity of neuraminidase determines the pathogenicity of influenza A virus.** *J Virol* 2001, **75**:9297–9301.
80. Yoneyama M, Suhara W, Fukuhara Y, Sato M, Ozato K, Fujita T: **Autocrine amplification of type I interferon gene expression mediated by interferon stimulated gene factor 3 (ISGF3).** *J Biochem* 1996, **120**:160–169.

doi:10.1186/1743-422X-9-106
Cite this article as: Wang *et al.*: PA from an H5N1 highly pathogenic avian influenza virus activates viral transcription and replication and induces apoptosis and interferon expression at an early stage of infection. *Virology Journal* 2012 **9**:106.

Self-Enhancement of Hepatitis C Virus Replication by Promotion of Specific Sphingolipid Biosynthesis

Yuichi Hirata[1], Kazutaka Ikeda[2,3], Masayuki Sudoh[4], Yuko Tokunaga[1], Akemi Suzuki[5], Leiyun Weng[6], Masatoshi Ohta[3], Yoshimi Tobita[1], Ken Okano[7], Kazuhisa Ozeki[7], Kenichi Kawasaki[4], Takuo Tsukuda[4], Asao Katsume[4], Yuko Aoki[4], Takuya Umehara[1], Satoshi Sekiguchi[1], Tetsuya Toyoda[6], Kunitada Shimotohno[8], Tomoyoshi Soga[3], Masahiro Nishijima[9,10], Ryo Taguchi[2,11], Michinori Kohara[1]*

1 Department of Microbiology and Cell Biology, Tokyo Metropolitan Institute of Medical Science, Setagaya-ku, Tokyo, Japan, **2** Department of Metabolome, Graduate School of Medicine, The University of Tokyo, Bunkyo-ku, Tokyo, Japan, **3** Institute for Advanced Biosciences, Keio University, Kakuganji, Tsuruoka, Yamagata, Japan, **4** Kamakura Research Laboratories, Chugai Pharmaceutical Co., Ltd., Kamakura, Kanagawa, Japan, **5** Institute of Glycoscience, Tokai University, Hiratsuka-shi, Kanagawa, Japan, **6** Unit of Viral Genome Regulation, Institut Pasteur of Shanghai, Key Laboratory of Molecular Virology & Immunology, Chinese Academy of Sciences, Shanghai, China, **7** Fuji-Gotemba Research Laboratories, Chugai Pharmaceutical Co., Ltd., Gotemba, Shizuoka, Japan, **8** Research Institute, Chiba Institute of Technology, Narashino, Chiba, Japan, **9** National Institute of Health Sciences, Setagaya-ku, Tokyo, Japan, **10** Showa Pharmaceutical University, Machidashi, Tokyo, Japan, **11** Department of Biomedical Sciences, College of Life and Health Sciences, Chubu University, Kasugai-shi, Aichi, Japan

Abstract

Lipids are key components in the viral life cycle that affect host-pathogen interactions. In this study, we investigated the effect of HCV infection on sphingolipid metabolism, especially on endogenous SM levels, and the relationship between HCV replication and endogenous SM molecular species. We demonstrated that HCV induces the expression of the genes (*SGMS1* and *2*) encoding human SM synthases 1 and 2. We observed associated increases of both total and individual sphingolipid molecular species, as assessed in human hepatocytes and in the detergent-resistant membrane (DRM) fraction in which HCV replicates. SGMS1 expression had a correlation with HCV replication. Inhibition of sphingolipid biosynthesis with a hepatotropic serine palmitoyltransferase (SPT) inhibitor, NA808, suppressed HCV-RNA production while also interfering with sphingolipid metabolism. Further, we identified the SM molecular species that comprise the DRM fraction and demonstrated that these endogenous SM species interacted with HCV nonstructural 5B polymerase to enhance viral replication. Our results reveal that HCV alters sphingolipid metabolism to promote viral replication, providing new insights into the formation of the HCV replication complex and the involvement of host lipids in the HCV life cycle.

Citation: Hirata Y, Ikeda K, Sudoh M, Tokunaga Y, Suzuki A, et al. (2012) Self-Enhancement of Hepatitis C Virus Replication by Promotion of Specific Sphingolipid Biosynthesis. PLoS Pathog 8(8): e1002860. doi:10.1371/journal.ppat.1002860

Editor: Aleem Siddiqui, University of California, San Diego, United States of America

Received January 4, 2012; **Accepted** June 27, 2012; **Published** August 16, 2012

Funding: This study was supported by grants from the Ministry of Education, Culture, Sports, Science, and Technology of Japan; the Program for Promotion of Fundamental Studies in Health Science of the National Institute of Biomedical Innovation of Japan; and the Ministry of Health, Labor, and Welfare of Japan. The funders had no role in study design, data collection and analysis, decision to publish, or preparation of the manuscript.

Competing Interests: M. Sudoh, A. Katsume, K. Okano, K. Ozeki, K. Kawasaki, T. Tsukuda, and Y. Aoki are employees of Chugai Pharmaceutical Co. Ltd. This does not alter our adherence to all PLoS Pathogens policies on sharing data and materials.

* E-mail: kohara-mc@igakuken.or.jp

Introduction

Lipids have long been known to play dual roles in biological systems, functioning in structural (in biological membranes) and energy storage (in cellular lipid droplets and plasma lipoproteins) capacities. Research over the past few decades has identified additional functions of lipids related to cellular signaling, microdomain organization, and membrane traffic. There are also strong indications of the important role of lipids in various stages of host-pathogen interactions [1].

Sphingomyelin (SM) is a sphingolipid that interacts with cholesterol and glycosphingolipid during formation of the raft domain, which can be extracted for study as a detergent-resistant membrane (DRM) fraction [2]. Recently, raft domains have drawn attention as potential platforms for signal transduction and pathogen infection processes [3,4]. For instance, raft domains may serve as sites for hepatitis C virus (HCV) replication [5,6]. Additionally, *in vitro* analysis indicates that synthetic SM binds to the nonstructural 5B polymerase (RdRp) of HCV [7]. This association allows RdRp to localize to the DRM fraction (known to be the site of HCV replication) and activates RdRp, although the degree of binding and activation differs among HCV genotypes [7,8]. Indeed, suppression of SM biosynthesis with a serine palmitoyltransferase (SPT) inhibitor disrupts the association between RdRp and SM in the DRM fraction, resulting in the suppression of HCV replication [7,9].

Multiple reports have indicated that HCV modulates lipid metabolism (e.g., cholesterol and fatty acid biosynthesis) to promote viral replication [10–12]. However, the effect of HCV infection on sphingolipid metabolism, especially on endogenous SM levels, and the relationship between HCV replication and endogenous SM molecular species remain to be elucidated as there are technical challenges in measuring SM levels (for both total and individual molecular species) in hepatocytes.

To address these questions, we first utilized mass spectrometry (MS)-based techniques and analyzed uninfected and HCV-

Author Summary

One of the key components for hepatitis C virus (HCV) propagation is lipids, some of which comprise membranous replication complexes for HCV replication. Research on cofactors that are involved in the formation of the membranous replication complex has advanced steadily; on the other hand, the lipids constituting the membranous replication complex remain to be elucidated. Here, we report that HCV modulates sphingolipid metabolism by promoting sphingolipid biosynthesis, to enhance viral replication. Specifically a specific molecular species of sphingomyelin (SM), a type of sphingolipid interacts with HCV nonstructural 5B polymerase, enhancing HCV replication. This work highlights the relationship between specific molecular species of SMs and HCV replication, giving new insight into the formation of the HCV replication complex and the involvement of host lipids in the HCV life cycle.

infected chimeric mice harboring human hepatocytes. Second, we developed a hepatotropic SPT inhibitor, NA808, and used this tool to elucidate the effects of inhibition of sphingolipid biosynthesis on hepatocyte SM levels. Third, we tested the inhibitor's anti-HCV activity in humanized chimeric mice, and demonstrated the relationship between HCV and endogenous SM in human hepatocytes. Finally, we identified the endogenous SM molecular species carried by the DRM fraction, defining the association between these molecular species and HCV replication.

Results

HCV upregulates SM and ceramide levels in hepatocytes of humanized chimeric mice

First, we examined the effects of HCV infection on SM biosynthesis in hepatocytes using humanized chimeric mice. The study employed a previously described mouse model (SCID/uPA) into which human hepatocytes were transplanted (see Materials and Methods). The average substitution rate of the chimeric mouse livers used in this study was over 80% [13], and HCV selectively infected human hepatocytes. This model supports long-term HCV infections at clinically relevant titers [13,14]. Indeed, the HCV-RNA levels reached (at 4 weeks post-infection) 10^8–10^9 copies/mL in the genotype 1a group (**Figure 1A**) and 10^6–10^7 copies/mL in the genotype 2a group (**Figure 1B**).

Once serum HCV-RNA levels had plateaued, we observed elevated expression of the genes (*SGMS1* and *2*) encoding human SM synthases 1 and 2; this pattern was HCV-specific, as demonstrated by the fact that the increase was not seen in hepatitis B virus-infected mice (**Figure 1C and Figure S1**). SM synthases convert ceramide to SM, so we next examined SM and ceramide levels in hepatocytes of both HCV-infected and uninfected chimeric mice. SM and ceramide levels were assessed using MS spectrometry, which allows analysis of samples at the single lipid species level as well as at the whole lipidome level. MS analysis showed that the level of ceramide, the precursor to SM, was increased in hepatocytes obtained from chimeric mice infected with HCV of either genotype (**Figure 1D**). Further, MS analysis showed that infection of chimeric mice with HCG9 (genotype 1a) was associated with increased SM levels in hepatocytes (**Figure 1E**). Similarly, SM levels were elevated in the hepatocytes of HCR24 (genotype 2a)-infected chimeric mice. These results indicate that infection with HCV increases total SM and ceramide levels in human hepatocytes.

MS analysis was conducted to determine which of several molecular species of SM [15] are present in HCV-infected hepatocytes. SM molecular species were analyzed in extracts obtained from a human hepatocyte cell line (HuH-7 K4) and from hepatocytes derived from the humanized chimeric mice. We identified four major peaks as SM molecular species (*d*18:1-16:0, *d*18:1-22:0, *d*18:1-24:0, and *d*18:1-24:1), and other peaks as phosphatidylcholine (**Figure 1F**). Infection-associated increases were seen for all ceramide molecular species, with significant changes in three of four species (excepting *d*18:1-16:0; $p<0.05$) with genotype 1a, and in all four species with genotype 2a ($p<0.05$) (**Figure 1G**). Upon infection with HCV of either genotype, hepatocytes tended to show increased levels of all four identified SM molecular species, but the changes were significant only for one species (*d*18:1-24:1; $p<0.05$) in genotype 1a and for two species (*d*18:1-16:0 and *d*18:1-24:1; $p<0.01$) in genotype 2a (**Figure 1H**). In cell culture, negligible amount of SM was likely increased by HCV infection. With respect to each molecular species, d18:1-16:0 SM was likely increased by HCV infection (**Figure S2**). These results indicate that HCV infection increases the abundance of several SM and ceramide molecular species.

Relationship between the SGMS genes and HCV infection

To clarify the relationship between SGMS1/2 and HCV, we investigated the correlation between SGMS1/2 expression and liver HCV-RNA in humanized chimeric mice. We found that SGMS1, but not SGMS2, had a correlation with liver HCV-RNA in HCV-infected humanized chimeric mice (**Figures 2A and 2B**).

Next, to clarify whether HCV infection of human hepatocytes increases the expression of the genes (*SGMS1* and *SGMS2*), we examined the effect of silencing HCV genome RNA on the expression of these genes in HCV-infected cells (**Figures 2C and 2D**). We found that silencing the HCV genome RNA decreases the expression of *SGMS1* and *SGMS2*.

The above results motivated us to examine the relationship between SGMS1/2 and HCV replication. Therefore, we examined the effect of SGMS1/2 mRNA silencing on HCV replication using subgenomic replicon cells [7,16]. We observed that silencing SGMS1 mRNA suppressed HCV replication, whereas silencing SGMS2 mRNA had no such effect (**Figures 2E and 2F**). These results indicate that SGMS1 expression has a correlation with HCV replication.

Characterization of the hepatotropic SPT inhibitor NA808

Based on our data, we hypothesized that HCV might alter the metabolism of sphingolipids, providing a more conducive environment for progression of the viral life cycle. To explore the relationship between HCV and sphingolipids, we investigated the effect of sphingolipid biosynthesis inhibition on HCV and the lipid profiles of SM and ceramide using HCV-infected chimeric mice harboring human hepatocytes. To inhibit the biosynthesis of sphingolipids, we used NA808, a chemical derivative of NA255, which is an SPT inhibitor derived from natural compounds [7]. We found that NA808 (**Figure 3A**) suppressed both the activity of SPT (**Figure 3B**) and biosynthesis of sphingolipids (**Figure 3C**) in a dose-dependent manner.

The conventional SPT inhibitor myriocin is not clinically beneficial due to immunosuppression through restriction of T-cell proliferation [17,18]. However, NA808 showed little immunosuppressive effect at the concentration at which NA808 suppressed HCV replication (**Figures 3D and 3E**). Moreover, pharmacokinetic analysis using [^{14}C]-labeled NA808 in rat models showed

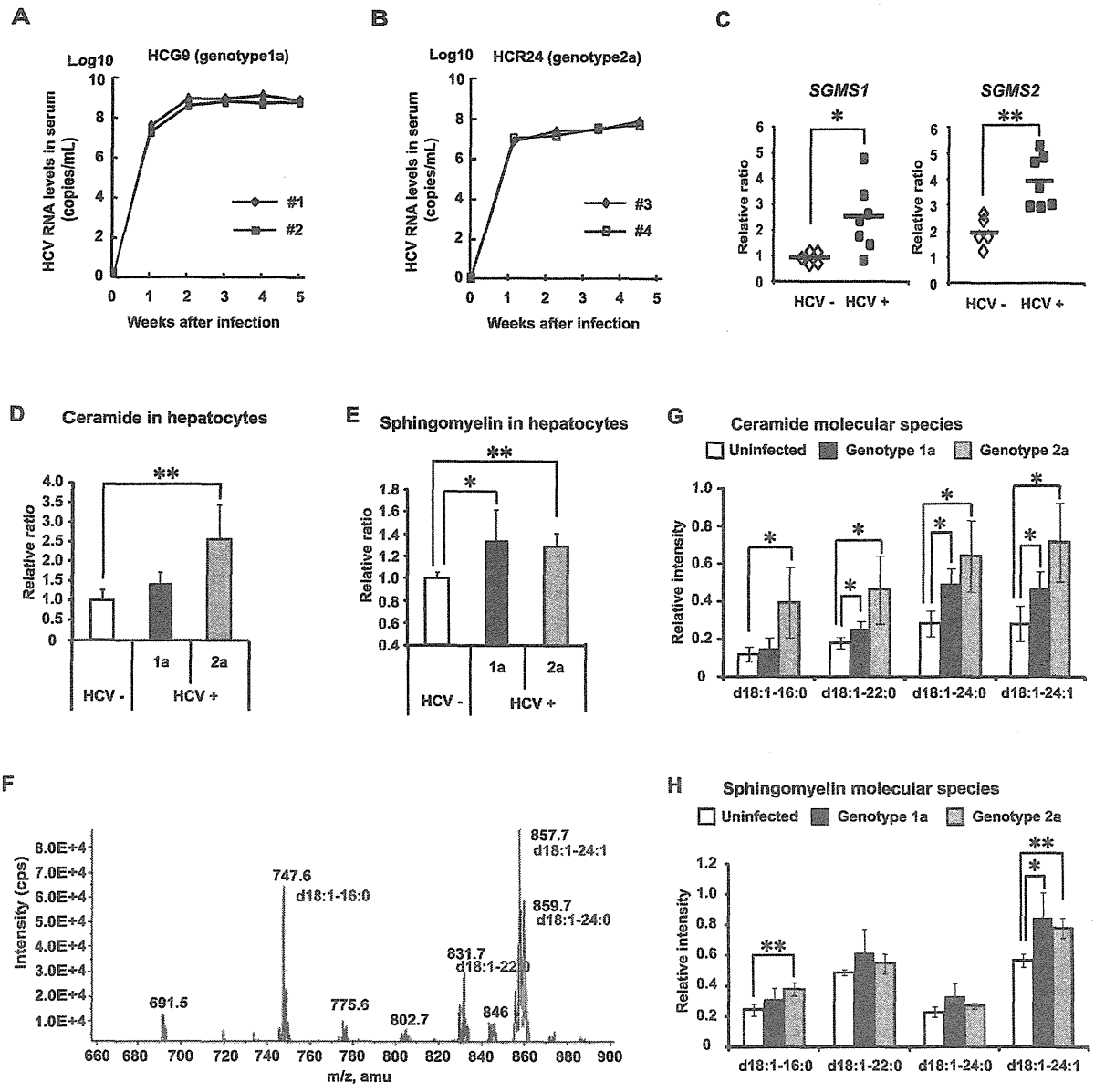

Figure 1. HCV alters sphingolipid metabolism. (**A, B**) Time-course studies of humanized chimeric mice inoculated with human serum samples positive for HCV genotype 1a (**A**) or 2a (**B**). (**C**) mRNA expression of *SGMS1* and *SGMS2* in uninfected (white, n = 5) and HCV genotype 1a-infected (black, n = 7) chimeric mice. (**D, E**) Effects of HCV infection on hepatocyte SM and ceramide levels in humanized chimeric mice. Relative intensity of total ceramide (**D**) and total shingomyelin (SM) (**E**) in uninfected mouse hepatocytes (white bar, n = 4), HCV genotype 1a-infected mouse hepatocytes (black bar, n = 5), and HCV genotype 2a-infected mouse hepatocytes (dark gray bar, n = 3). (**F**) Mass spectrum of SM in Bligh & Dyer extracts of a human hepatocyte cell line (HuH-7 K4). (**G, H**) Effects of HCV infection on hepatocyte SM and ceramide levels in humanized chimeric mice. Relative intensity of individual ceramide molecular species (**G**) and individual SM molecular species (**H**) in uninfected mouse hepatocytes (white bar, n = 3), HCV genotype 1a-infected mouse hepatocytes (black bar, n = 3), and HCV genotype 2a-infected mouse hepatocytes (dark gray bar, n = 3). In all cases, error bars indicate SDs. *$p<0.05$ and **$p<0.01$ compared with uninfected hepatocytes.
doi:10.1371/journal.ppat.1002860.g001

that NA808 mainly accumulated in the liver and small intestine (**Table S1**). These results indicate that NA808 suppressed SPT activity, with hepatotropic and low immunosuppressive properties.

Based on these results, we then examined the effects of inhibition of sphingolipid biosynthesis with NA808 on HCV replication using subgenomic replicon cells [7,16]. The luciferase activity of FLR3-1 showed that replication was suppressed by NA808 in a dose-dependent manner with no effect on cell viability, as measured by the WST-8 assay (**Figure 3E**). Similarly, western blot and immunofluorescence analysis showed that NA808 effectively suppressed HCV replication (**Figures 3F and 3G**).

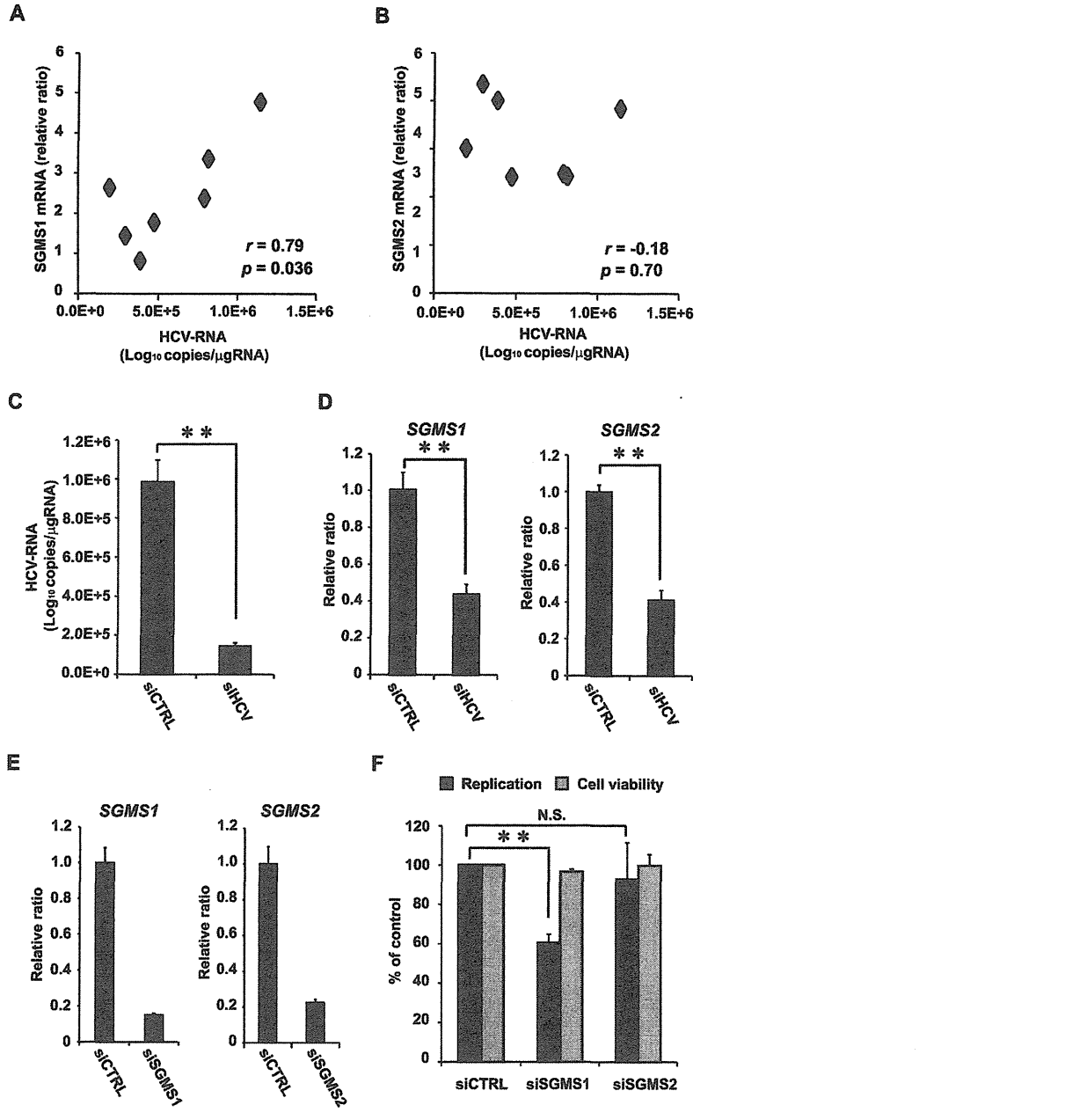

Figure 2. Relationship between the SGMS genes and HCV infection. (**A, B**) The correlation between SGMS1/2 and liver HCV-RNA of HCV infected humanized chimeric mice (n = 7). (**C**) The effect of silencing HCV genome RNA with siRNA (siE-R7: 1 nM) on HCV in HCV-infected cells. (**D**) The effect of silencing HCV genome RNA with siRNA (siE-R7: 1 nM) on the expression of SGMS1/2 mRNA measured by RTD-PCR. (**E**) The effect of silencing SGMS1/2 mRNA with siRNA (3 nM each) measured by RTD-PCR. (**F**) The effect of silencing SGMS1/2 mRNA with siRNA (3 nM) on HCV replication in FLR 3-1. In all cases, error bars indicate SDs. *$p<0.05$ and **$p<0.01$.
doi:10.1371/journal.ppat.1002860.g002

Inhibition of sphingolipid biosynthesis impedes HCV infection of chimeric mice

To evaluate the effects of inhibition of sphingolipid biosynthesis in an animal model, we administered NA808 or pegylated interferon-α (PegIFN-α) via intravenous or subcutaneous injection to HCV-infected chimeric mice harboring human hepatocytes (**Table S2**). In chimeric mice infected with HCV genotype 1a, NA808 treatment led to a rapid decline in serum HCV-RNA (approximately 2–3 log units within 14 days). On the other hand, PegIFN-α produced less than a 1 log unit reduction, despite being delivered at 20 times the typical clinical dose (**Figure 4A**). Furthermore, results of 21-day NA808 treatment (5 mg/kg) in individual mice indicated that serum HCV RNA continued to decrease in all chimeric mice without viral breakthrough

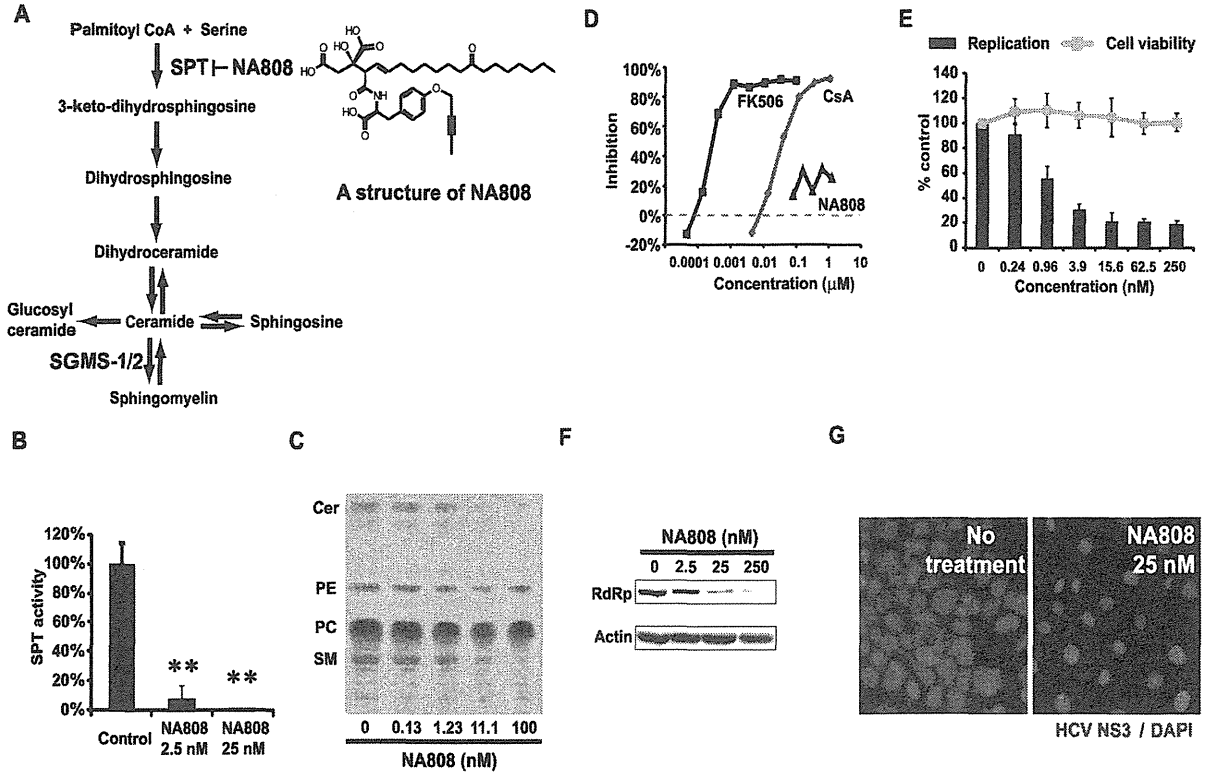

Figure 3. Characterization of the hepatotropic serine palmitoyltransferase inhibitor NA808. (**A**) Sphingolipid biosynthesis pathway and structure of NA808. (**B**) Activity of SPT in FLR3-1 cells after 72 h of NA808 treatment. $^{**}p<0.01$ compared with control. (**C**) Results of TLC showing *de novo* sphingolipid biosynthesis in the presence of NA808. Cer = ceramide, PE = phosphatidylethanolamine, PC = phosphatidylcholine, SM = sphingomyelin. (**D**) Immunosuppressive activity of NA808. Cyclosporin A (CsA) and tacrolimus (FK-506) were used as positive controls. (**E**) Effects of NA808 on HCV replication (black bars) and cell viability (gray symbols) in FLR 3-1 replicon-containing cells. Error bars indicate SDs. (**F**) Effects of NA808 on the level of the RdRp and β-actin, as assessed by Western blotting. (**G**) Effect of NA808 on the production of HCV NS3 protein (green) in FLR3-1 replicon-containing cells, as assessed by immunofluorescence analysis. Nuclear DNA was stained with DAPI (blue).
doi:10.1371/journal.ppat.1002860.g003

(**Figure 4B**). Notably, in 2 of 5 chimeric mice, serum HCV-RNA was not detectable at the end of the 21-day regimen. Consistent with this observation, the levels of both hepatic HCV-RNA and HCV core protein decreased significantly ($p<0.01$ and $p<0.05$, respectively) following NA808 treatment, these effects being dose dependent (**Figure 4C**). Immunofluorescence analysis and immunohistochemistry confirmed the reduced abundance of HCV core protein after 14 days of treatment (**Figure 4D and Figure S3**).

In genotype 2a-infected chimeric mice, NA808 decreased serum HCV-RNA by approximately 3 log units within 14 days (**Figure 4E**). NA808-treated mice displayed a corresponding reduction in hepatic HCV-RNA (**Figure 4F**). NA808 did not affect body weight or human serum albumin levels (**Figures S4A and S4B**). Furthermore, hematoxylin and eosin (H&E) staining revealed little morphological change in response to treatment with NA808. Immunofluorescence analysis also indicated that NA808 did not affect the production of human albumin (**Figure S4C**). Thus, inhibition of sphingolipid biosynthesis by an SPT inhibitor impeded HCV replication in an animal infection model, regardless of HCV genotype.

Inhibition of SPT decreases ceramide and SM levels in hepatocytes of humanized chimeric mice

We next investigated the effects of sphingolipid biosynthesis inhibition on SM and ceramide levels in hepatocytes of humanized chimeric mice. Pharmacokinetic analysis in a rat model indicated that NA808 has hepatotropic properties (**Table S1**). Consistent with this analysis, our study in chimeric mice also indicated that the NA808 concentration was much higher in the liver than in serum (**Figure S5**). Furthermore, we observed that serum SM content was not decreased by NA808 treatment (**Figure S6**), in contrast to the effects previously observed for myriocin, another SPT inhibitor [19].

In HCV-infected chimeric mouse hepatocytes, MS analysis indicated that HCV infection resulted in increased ceramide and SM levels. However, treatment of infected animals with NA808 (5 mg/kg) attenuated this increase in ceramide and SM levels in hepatocytes, and the change in SM was significant ($p<0.05$) compared to the level observed in HCV-infected chimeric mice with no treatment. This effect of NA808 on ceramide and SM levels was dose-dependent (**Figures 5A and 5B**). We also found that SM levels and hepatic HCV-RNA were correlated (**Figure 5C**).

Interestingly, treatment with NA808 effectively decreased two specific SM and ceramide molecular species (*d*18:1-22:0 and *d*18:1-24:0), slightly decreased one other species (*d*18:1-24:1), and hardly decreased another (*d*18:1-16:0). Further, we found that among SM and ceramide molecular species, *d*18:1-16:0 did not change (**Figures 5D and 5E**). These results indicate that the

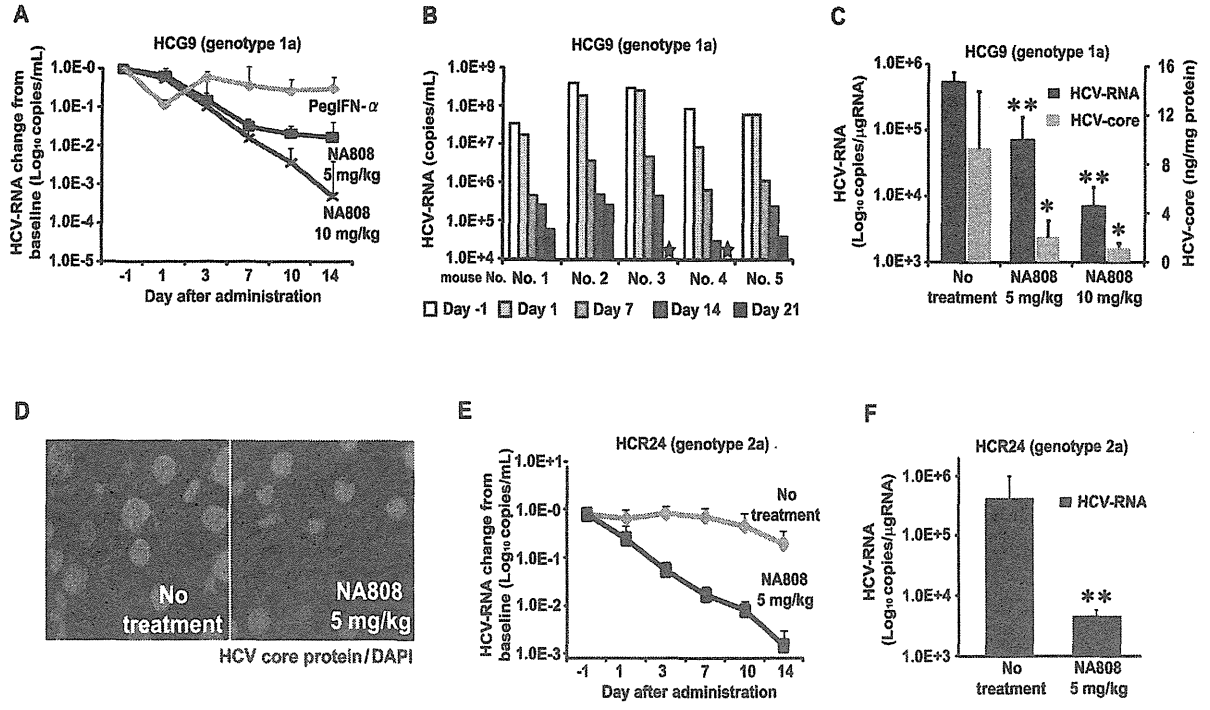

Figure 4. Inhibition of sphingolipid biosynthesis with hepatotropic serine palmitoyltransferase (SPT) inhibitor NA808 exerts anti-HCV effect. (**A**) Serum HCV-RNA levels in response to treatment with NA808 (blue, 5 mg/kg/day, purple, 10 mg/kg/day, n = 6 each), or PegIFN-α (pink, 30 μg/kg twice weekly, n = 4). (**B**) Effect of NA808 (5 mg/kg/day) on serum HCV-RNA levels. A star indicates that HCV-RNA was not detected. (**C**) Levels of liver HCV-RNA (black) and HCV core protein (gray) after the 14-day treatment. *$p<0.05$ and **$p<0.01$ compared with no treatment. (**D**) Histological analysis using immunofluorescent labeling of HCV core protein (green) and fluorescent staining of nuclei (blue). (**E**) Serum HCV-RNA levels in response to no treatment (pink, n = 3) or NA808 treatment (blue, 5 mg/kg/day, n = 4). (**F**) Liver HCV-RNA levels in genotype 2a-infected mice after the 14-day treatment. *$p<0.05$ and **$p<0.01$ compared with no treatment. In all cases, error bars indicate SDs.
doi:10.1371/journal.ppat.1002860.g004

effects of sphingolipid biosynthesis inhibition varied among the molecular species.

Considering these results, we found a discrepancy in SM molecular species which were considered to be important for HCV replication. To elucidate the relationship between SM molecular species and HCV replication, we attempted to identify endogenous SM molecular species comprising the DRM fraction and to evaluate the effects of HCV infection and inhibition of sphingolipid biosynthesis on SM levels of the DRM.

Relationship between endogenous SM molecular species constituting the DRM and HCV replication

We previously reported that SM interacts with RdRp, allowing it to localize to the DRM fraction where HCV replicates and activates RdRp [7,8], and that suppression of SM biosynthesis disrupts the association between RdRp and SM in the DRM fraction, resulting in suppression of HCV replication [7,8]. In the present study, treatment with NA808 decreased SM levels in the DRM fraction; the decreased presence of SM correlated with decreased RdRp abundance, but the same effect was not seen for HCV nonstructural protein 3 (**Figures S7A–C**). Given these results, we investigated whether HCV replication was induced by elevated SM levels. Specifically, we compared SM levels in the DRM fraction between HCV-infected hepatocytes and uninfected hepatocytes. MS analysis showed that HCV increased SM levels in the DRM fraction more remarkably than in whole cells (**Figure 6A**). Next, we identified SM molecular species composing the DRM fraction and found that the composition ratio of SM molecular species was distinct between whole cells and DRM fractions in both HCV-infected and uninfected hepatocytes (**Figure 6B and Figure S8**). The DRM was composed primarily (69%) of *d*18:1-16:0, followed (in decreasing order) by *d*18:1-24:0, *d*18:1-22:0, and *d*18:1-24:1; the abundance of all SM molecular species increased upon HCV infection (**Figure 6C**). Further, NA808 treatment decreased all SM molecular species in the DRM fraction. Consistently, NS3 protease inhibitor decreased all SM molecular species in the DRM fraction of subgenomic replicon cells (**Figure S9**).

To address the association between RdRp and the endogenous SM molecular species composing the DRM, we used high-performance liquid chromatography (HPLC) to separate each SM molecular species from bulk SM derived from bovine milk and brain. We evaluated the relationship between RdRp and these endogenous SM molecular species using *in vitro* analysis. Enzyme-linked immunosorbent assay (ELISA) indicated that these endogenous SM molecular species bound to RdRp more readily than the bulk SM derived from milk as a positive control (**Figure 6D**). Further, *in vitro* HCV transcription analysis showed that three SM species (*d*18:1-16:0, *d*18:1-22:0, and *d*18:1-24:1) increased *in vitro* RdRp activation by approximately 5-fold, whereas the *d*18:1-24:0 species increased activation by 2-fold (**Figure 6E**). In a previous study, the soluble RdRp without its C-terminal hydrophobic 21-amino-acid sequence was used in *in vitro* analysis [8], and whether the relationship between RdRp and SM proved in this analysis

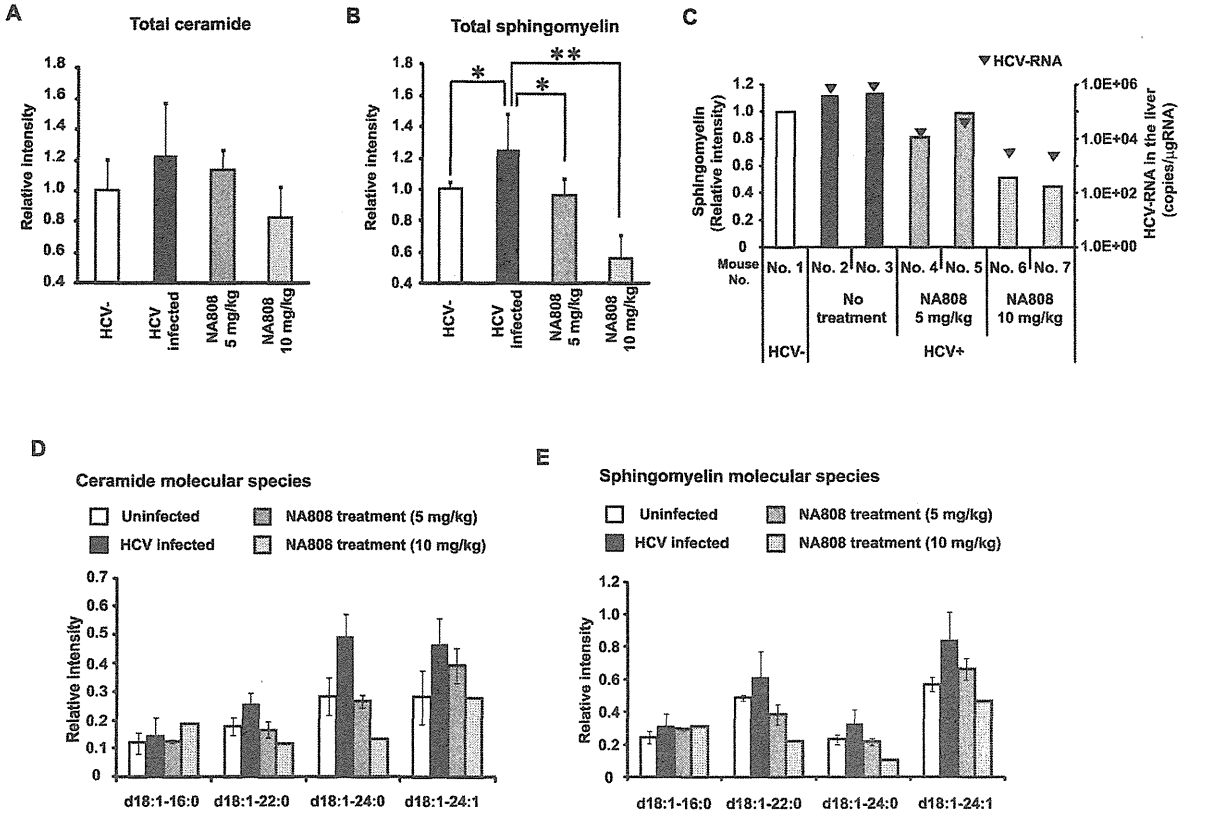

Figure 5. Effects of NA808 treatment on sphingomyelin (SM) and ceramide (total and individual molecular species). (**A, B**) Relative ratio of total ceramide (**A**) and SM (**B**) in uninfected mice (white, n = 4), HCV genotype 1a-infected mice (black, n = 5), and HCV-infected mice treated with NA808 for 14 days (dark gray, 5 mg/kg, n = 4; light gray, 10 mg/kg, n = 3). *$p<0.05$ and **$p<0.01$ compared with HCV-infected mice. (**C**) SM levels (bars) and HCV RNA levels (black arrowhead) in the livers of mice treated for 14 days with NA808 (5 or 10 mg/kg/day) and untreated chimeric mice. (**D, E**) Relative intensities of individual ceramide molecular species (**D**) and individual SM molecular species (**E**) in uninfected mice (white, n = 3), HCV-infected mice (black, n = 3), and HCV-infected mice treated with NA808 for 14 days (dark gray, 5 mg/kg, n = 2; light gray, 10 mg/kg, n = 1). In all cases, error bars indicate SDs.
doi:10.1371/journal.ppat.1002860.g005

reflected the state in the membranous replication complex remains to be elucidated. Therefore, we attempted to examine the effect of endogenous SM molecular species on HCV replicase activity *in vivo* using digitonin-permeabilized semi-intact replicon cells, which permit monitoring of the function of the active HCV replication complex (**Figure 6F**) [20]. This *in vivo* analysis also enabled us to deliver the extrinsically added SM molecular species directly to the cytosol. This RNA replication assay indicated that the endogenous SM molecular species (*d*18:1-16:0 and *d*18:1-24:0) enhanced HCV-RNA replication, these species being consistent with the two SM molecular species that primarily constitute the DRM and are decreased significantly by NA808 treatment (**Figures 6G and 6H**). These results suggest that HCV infection modifies the levels of specific endogenous SM molecular species, which in turn enhance HCV-RNA replication by interacting with RdRp.

Discussion

In this study, we showed that HCV alters sphingolipid metabolism, resulting in a better environment for viral replication. Specifically, HCV increased SM content in the DRM fraction; this step is essential for viral replication since SM is a key component of the membranous replication complex and interacts with RdRp. Employing MS analysis, we identified endogenous SM molecular species (located in the DRM fraction) that increased upon HCV infection, and demonstrated that these endogenous SM molecular species interact directly with RdRp, enhancing HCV replication. Thus, we concluded that HCV modulates sphingolipid metabolism to promote viral replication.

We found that the expression levels of SGMS1/2 and the content of SM and ceramide in HCV-infected humanized chimeric mouse livers was increased (Figure 1). Our measurement revealed that chronic HCV infection promoted sphingolipid biosynthesis. HCV is known to induce cellular stress [21,22]. A variety of cell stressors increase intracellular ceramide content during the execution phase of apoptosis [23,24], indicating that ceramide is a proapoptotic lipid mediator. Furthermore, activation of ceramide-metabolizing enzymes such as glucosylceramide synthase and SM synthase can attenuate apoptosis by decreasing the intracellular ceramide content [25,26]. We found that HCV infection correlated with increased mRNA levels of the genes that encode human SM synthases (*SGMS1/2*) and glucosylceramide synthase (*UGCG*) (data not shown). Thus, the increase in ceramide levels observed in our study was likely to activate enzymes that transfer ceramide to other sphingolipids. On the other hand, Diamond et al. reported on lipidomic profiling performed over the